International Journal of Applied Earth Observation and Geoinformation 143 (2025) 104783

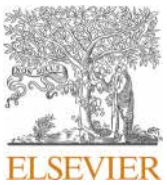

Contents lists available at ScienceDirect

International Journal of Applied Earth Observation and Geoinformation

journal homepage: www.elsevier.com/locate/jag

Fire Impacts, vegetation Recovery, and environmental drivers in West African savannas (2014–2023): A High-Resolution remote sensing assessment

Boris Ouattara [a], Michael Thiel [b,*], Gerald Forkuor [c], Florent Mouillot [d], Paul Laris [e], Ebagnerin Jérôme Tondoh [f], Barbara Sponholz [g]

[a] Institute of Climate-Smart Agriculture, Thuenen Institute, 38116 Brunswick, Germany
[b] University of Würzburg, Institute of Geography and Geology, Department of Remote Sensing, John Skilton Str. 4a, 97074 Würzburg, Germany
[c] Center for Earth Observation and Environmental Research, Accra, Ghana
[d] UMR CEFE 5175, Centre National de la Recherche Scientifique, Université de Montpellier, Université Paul-Valéry Montpellier, Ecole Pratique des Hautes Etudes, Institut de Recherche pour le Développement, 1919 route de Mende, 34293 Montpellier Cedex 5, France
[e] Department of Geography, California State University Long Beach 1250 Bellflower Blvd, Long Beach, CA 90840, USA
[f] Department of Natural Sciences. Ecology and Sustainable Development Laboratory (LEDD), Nangui Abrogoua University, 02 BP 801 Abidjan 02, Côte d'Ivoire
[g] University of Würzburg, Institute of Geography and Geology, Department of Physical Geography, Am Hubland 2, 97074 Würzburg, Germany

ARTICLE INFO

Keywords:
Burned area
Net primary productivity
Post-fire recovery
Machine learning
Harmonized Landsat-Sentinel-2
Savanna fires
West Africa

ABSTRACT

Savanna fires are a dominant ecological force in West Africa, shaping land systems, carbon dynamics, and biodiversity. Yet, their impacts on ecosystem productivity and recovery remain poorly quantified at meaningful spatial and temporal scales. This study presents a decadal assessment (2014–2023) of fire activity and post-fire vegetation response across a ~ 229,000 km^2 transboundary region of Burkina Faso, Ghana, and Côte d'Ivoire. Using Harmonized Landsat–Sentinel (HLS) imagery and VIIRS active fire detections, we mapped burned areas (BA) at 30 m resolution—capturing extensive small fires often missed by global datasets. Fire-induced Net Primary Productivity (NPP) losses were estimated using downscaled MODIS productivity data, and post-fire recovery times were tracked at monthly and annual scales. Fires were highly seasonal, with > 80 % of BA occurring between November and January, peaking in December. Despite a dip around 2017, interannual BA remained relatively stable (0.29 % yr^{-1} increase, $p > 0.05$). Immediate NPP losses averaged ~ 11 × 10–2 Mg C ha^{-1} per year, with higher per-hectare losses in forested and high-biomass zones. Roughly 65 % of BA recovered to pre-fire NPP levels within a year, primarily in grasslands and croplands. However, recovery in woody and mesic areas was slower and more variable. We emphasize that recovery was assessed in terms of NPP (carbon uptake), not structural biomass or species composition—functional recovery does not necessarily imply full ecological recovery. Using machine learning, we identified soil moisture (dry-season NDMI) and temperature as dominant predictors of recovery time, with soil fertility (nitrogen content) and water retention capacity emerging as key drivers. Interestingly, fire frequency and land cover type had limited predictive power once climate and soil factors were accounted for, suggesting that environmental factors, more than fire regime characteristics, shape recovery. These findings support the idea that well-timed, low-intensity fires—particularly early-season burns—can promote carbon resilience in fire-adapted landscapes. This underscores the value of high-resolution remote sensing and soil data in guiding fire-smart management and balancing ecological and livelihood goals under climate change.

1. Introduction

Fire is a major ecological force in savanna landscapes and plays a critical role in the global carbon cycle. Tropical savannas, including those of West Africa, account for a substantial portion of the Earth's burned area (BA) and fire emissions. According to Giglio et al. (2016), Africa contributes approximately 70 % of global BA, while Van der Werf et al. (2017) estimate that the continent accounts for about 50 % of fire-

* Corresponding author.
E-mail address: michael.thiel@uni-wuerzburg.de (M. Thiel).

https://doi.org/10.1016/j.jag.2025.104783
Received 21 May 2025; Received in revised form 31 July 2025; Accepted 3 August 2025
Available online 6 August 2025

related carbon emissions. These figures highlight the global importance of African savannas for land–atmosphere interactions and global climate regulation.

In West Africa, fire regimes are shaped by a combination of biophysical conditions and long-standing human practices. Unlike many other tropical regions where fire may be mainly climate-driven, savanna fires here are largely anthropogenic, embedded in traditional land management and cultural practices (Caillault et al., 2020; Laris et al., 2023). Fire is often used to clear land, manage grazing, facilitate hunting, and maintain open landscapes. Such intentional burning contributes to a relatively predictable and spatially extensive fire regime (Devineau et al., 2010; Dahan et al., 2023). Laris et al. (2016) describe this as a "buffering fire regime," where frequent, early-season, low-intensity fires help prevent woody encroachment and sustain savanna structure. This aligns with the broader "fire-vegetation feedback" framework (Beckage and Ellingwood 2009; Hurteau et al., 2019; Gold et al., 2023), which posits that fire is not just a disturbance, but a structuring process maintaining the savanna state and preventing transitions toward forest.

Fire timing also plays a key ecological role. Early and mid-dry season fires are generally less intense and allow for rapid post fire regrowth, while late season fires, when fuels are dry and continuous, tend to be more severe and ecologically disruptive (N'Dri et al., 2012; N'Dri et al., 2022). Zoffoun et al. (2024) found that fire intensity peaks early in the dry season in West Africa, though this varies by vegetation and moisture conditions. Studies by Dwomoh and Wimberly (2017) and Amoako and Gambiza (2022) have demonstrated how land cover, fuel structure, and phenology influence fire frequency and behaviour, resulting in spatially heterogeneous burn patterns across the savanna-forest mosaic.

This ecological complexity is further enriched by the concept of pyrodiversity, i.e., variability in fire regimes over space and time. Pyrodiversity is increasingly recognized as a driver of biodiversity and ecosystem resilience (Beale et al., 2018; Jones and Tingley, 2021). Variation in fire return interval, patchiness, and intensity can create a mosaic of successional stages and resource availability, promoting species coexistence. However, excessive or poorly timed fires may reduce this diversity, especially in ecotonal areas where forest and savanna meet (Hoffmann et al., 2012; Pellegrini et al., 2016).

Despite the ecological importance of fire, its impact on ecosystem functioning, especially on primary productivity, remains poorly quantified at high spatial resolution in West Africa. Wildfires can cause immediate reductions in photosynthetic capacity by consuming biomass and damaging plant tissues (Fernández-García et al., 2018). Post-fire vegetation recovery is a key indicator of system functioning. In fire-adapted ecosystems, grasses and resprouting shrubs often recover within a single growing season (Tredennick et al., 2014), but in mesic or woody zones, recovery can be slower and more variable, depending on climate and disturbance history (Dikshit and Evans, 2024). Other biotic pressures, such as grazing, further shape post-fire dynamics: heavy herbivory can delay or redirect regrowth trajectories, sometimes favouring shrub encroachment (Roques et al., 2001; Thapa et al., 2022; Vincent et al., 2024).

At broader scales, climate and soil conditions strongly influence fire impacts and recovery. Rainfall amount and distribution govern vegetation structure and fuel loads, thereby modulating fire frequency and intensity (Devine et al., 2015; Huntley, 2023). Soil fertility, water retention capacity, and plant trait composition also influence post-fire regrowth rates and ecosystem trajectories (Hoffmann et al., 2012). The interaction of these factors makes West Africa savanna fire ecology highly context dependent, highlighting the need for regionally grounded studies.

Satellite remote sensing has revolutionized the monitoring of wildfires, providing consistent data on active fires and BA across large regions (Dezfuli et al., 2024). Coarse-resolution products from the Moderate Resolution Imaging Spectroradiometer (MODIS) sensor have enabled global fire trend analyses (Katagis and Gitas, 2022; Chen et al., 2023) and revealed a human-driven decline in BA over the past decades (Andela et al., 2017), including parts of Africa (e.g., due to agricultural expansion and fire suppression) (Forkel et al., 2019). In West Africa, however, fire remains a frequent disturbance, and traditional satellite products (500–1000 m) often under detect small fires that are prevalent in these savanna mosaics (Ramo et al., 2021). Recent advances in earth observation offer improved capabilities for wildfire studies. The Visible Infrared Imaging Radiometer Suite (VIIRS) sensor (375 m) and Sentinel-2 (10–20 m) provide higher resolution detection of fire activity and burned scars (Fu et al., 2020; Gaveau et al., 2021; Pinto et al., 2021). By combining data from multiple sensors, it is now possible to map BA at higher resolution, capturing fine-scale burn patterns that were previously missed (Filipponi, 2019). In addition to broad-scale monitoring, recent work has also shown that remote sensing can be effective at detecting and analysing fire effects in marginal or transitional zones, such as forest edges and ecotones (Rossetti et al., 2024; Calderisi et al., 2025). This granularity is crucial in heterogeneous West African landscapes, where burn scars are often small and patchy due to fragmented land cover and controlled burning practices (Laris, 2005).

In this study, we integrate multi-source satellite data to assess wildfire impacts on ecosystem productivity in West African savannas over a ten-year period (2014–2023). We aim to (1) generate a high-resolution BA dataset integrating VIIRS active fire detections and Harmonized Landsat-Sentinel-2 imagery, (2) quantify the immediate loss of net primary productivity (NPP) due to fire and its spatial variability across land cover types, (3) evaluate the post-fire recovery time of vegetation at monthly and annual scales, and (4) identify the environmental and biophysical drivers that influence recovery rates, using a machine learning approach. We define NPP loss in two ways: seasonal loss, as the short-term drop in carbon uptake following fire, and annual loss, as the difference in productivity between years before and after burning. Our analysis emphasizes functional recovery—the return of NPP—rather than structural recovery, which involves slower regrowth of biomass and canopy structure (Bond and Keeley, 2005). We use the term "recovery" to refer to the return of ecosystem productivity (measured via NPP) following fire. Where the term "functional resilience" is used, it specifically refers to the capacity of an ecosystem to regain its carbon uptake function (via NPP), without implying full structural or compositional restoration. By focusing on West Africa, a region with intense fire activity and diverse ecosystems, our study provides new insights into savanna fire dynamics. We further discuss the implications of our findings for fire management, carbon accounting, and biodiversity conservation in the context of climate change.

Understanding how fire affects NPP which represents the net carbon uptake by ecosystems, is central to our study. Immediately after a fire, NPP typically drops as photosynthetic capacity is reduced, and it can take months or years for productivity to return to pre-fire levels (Landi et al., 2020; Klupar et al., 2021). The length of this recovery period is a key indicator of ecosystem resilience (carbon resilience in terms of NPP recovery). Previous research has shown that post-fire recovery rates depend on fire intensity, vegetation type, and climate conditions such as rainfall availability (Tepley et al., 2018). In frequently burned savannas, grasses and resprouting shrubs may recover within a single growing season, whereas in less fire-adapted forests, canopy regeneration may require several years. However, there is limited quantitative data on recovery times in West African savannas across large spatial scales. Moreover, the drivers of recovery—whether primarily controlled by fire characteristics (frequency, seasonality, severity), vegetation properties, or external factors like moisture and temperature—are not fully understood in this region.

2. Study area

The study area encompasses a savanna region in West Africa spanning approximately 4.6° W to 1.7° E longitude and 8.5° N to 11.4° N latitude (Fig. 1). This rectangular region covers about 229,500 km^2, an area roughly equivalent to 71 % of Côte d'Ivoire's land surface or nearly

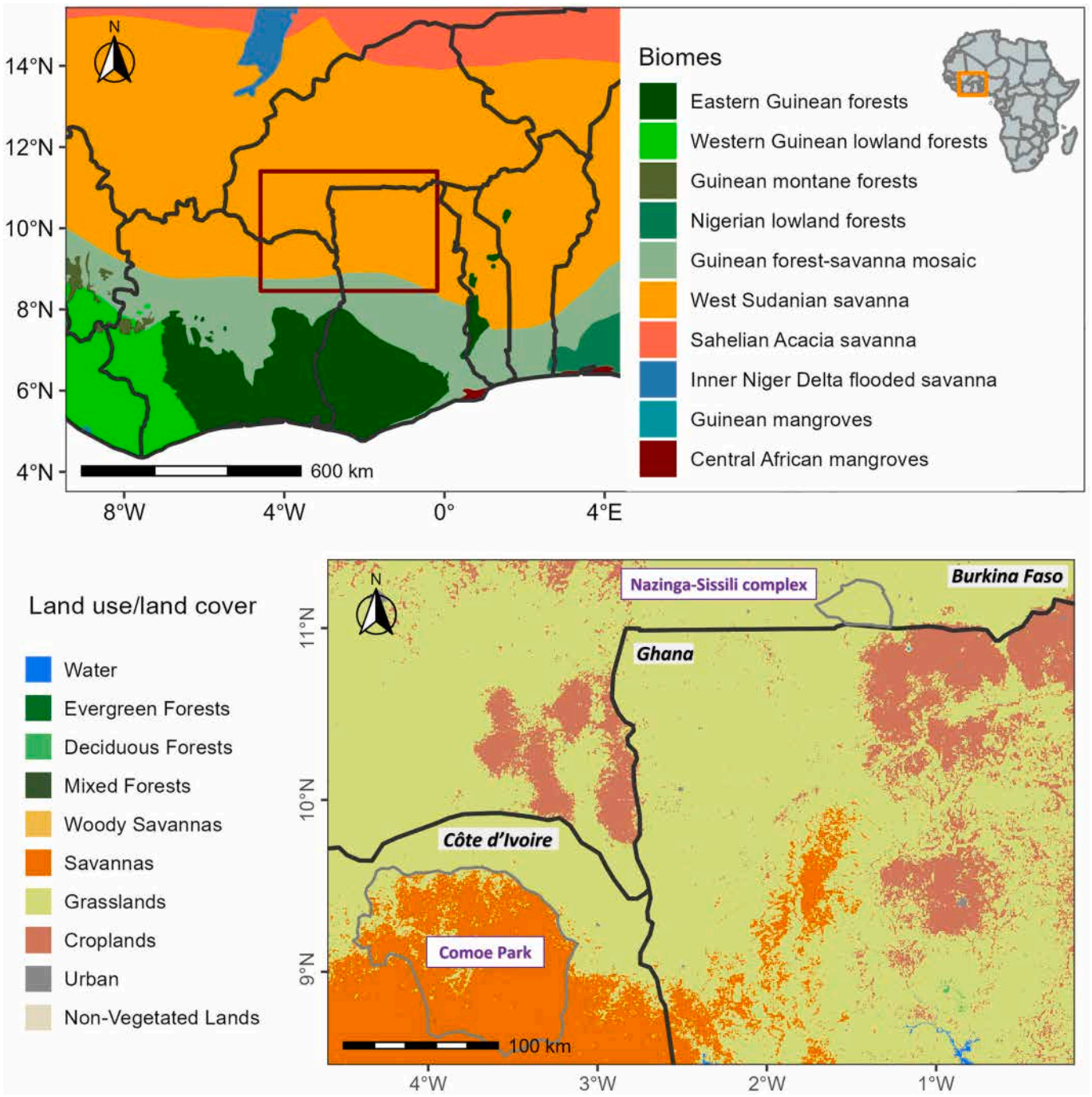

Fig. 1. Study area. The upper panel shows the West Sudanian Savanna and Guinean Forest-Savanna Mosaic ecoregions (Olson et al., 2001) and the lower panel the study area major land use and land cover according to the MCD12 dataset (Friedl and Sulla-Menashe, 2019).

the entirety of Ghana. It includes parts of southern Burkina Faso, northern Ghana, and north-eastern Côte d'Ivoire, intersecting diverse ecological zones and socio-economic landscapes. It spans a gradient from the West Sudanian savanna biome in the north to the Guinean forest–savanna mosaic in the south (as classified by Olson et al., 2001). This gradient includes semi-arid savannas where fire is more limited by fuel and rainfall, and mesic, fire-driven savannas in the south, where frequent burning suppresses woody encroachment and shapes vegetation structure (Sankaran et al., 2005; Higgins et al., 2007). Within these broad vegetation types, vegetation cover ranges from grass-dominated savannas and open woodlands to patches of deciduous and semi-evergreen forests embedded in the mosaic. This variety of land cover provides critical ecosystem services, including carbon sequestration, water regulation, and wildlife habitat.

Within the study region are areas of notable conservation importance. Comoé National Park in north-eastern Côte d'Ivoire (a UNESCO World Heritage Site) covers ~ 11,500 km2 and contains a rich tapestry of habitats—forests, savannas, and wetlands—that support high biodiversity (Koné et al., 2018). Its transitional location between forest and savanna makes Comoé particularly valuable for studying fire impacts on different vegetation types. Similarly, the Pô-Nazinga-Sissili complex (CAP/PONASI) in southern Burkina Faso is a large protected area and Ramsar wetland, harbouring diverse flora and fauna. This landscape includes fire-adapted savanna species such as Vitellaria paradoxa (shea tree) and Afzelia africana, as well as large mammals like elephants that move between Burkina Faso and Ghana (Zoungrana et al., 2023). Both

protected and unprotected lands in the region experience seasonal fires and serve as reference points for understanding natural vs. human-modified fire regimes. The area's strategic location and ecological diversity makes it highly relevant for understanding fire dynamics, carbon cycling, and vegetation recovery processes.

The climate is tropical with a unimodal rainfall pattern. A rainy season from roughly May to October brings annual precipitation of about 800 mm in the north to over 1200 mm in southern areas. A pronounced dry season from November to April features high temperatures (average daily 25–35 °C) and desiccated vegetation, creating conditions conducive to fire spread (Laris, et al., 2020). In this region, wildfires are most frequent during the early dry season, when accumulated grassy fuels and crop residues are ignited by farmers or natural causes. Indeed, fire is an ingrained component of local land management. It is used for clearing fields, hunting, and pasture renewal. While these fires are often set intentionally, they can escape control and burn extensive areas. Rural communities possess traditional knowledge for coping with wildfires like early dry season burns, firebreaks, and community fire brigades (Krawchuk and Moritz, 2011), but fire remains a significant risk to both livelihoods and biodiversity.

Widespread agriculture and grazing influence the fire regime. Outside protected areas, expanding croplands and shifting cultivation have led to land cover changes that may either increase or decrease fire occurrence. Deforestation, mostly as a result of farmland expansion tends to fragment the landscape, sometimes reducing the continuity of burnable fuels, but agricultural fires for clearing can add to overall fire numbers. Recent studies highlight rapid land-use change in parts of West Africa (Dimobe et al., 2018) and stress the need to balance agricultural development with ecosystem conservation. In our study area, regions around Dano (Burkina Faso) and Bolgatanga (Ghana) represent such human-dominated savannas where fire, farming, and grazing interact. In contrast, core zones of Comoé National Park and remote savanna woodlands experience more natural fire regimes, primarily driven by climate and fuel loads. This mix of conditions across the study area provides an ideal natural laboratory to investigate how fire impacts on productivity differ by land use and ecological context. Moreover, with climate change potentially altering rainfall patterns and drying trends in West Africa, examining historical fire-recovery dynamics offers insights into future ecosystem resilience under shifting fire frequencies and intensities. This rectangular extent was selected to maximize ecological representativeness by spanning key vegetation transitions, while also ensuring consistent spatial and temporal coverage across the HLS, MODIS, and VIIRS datasets from 2014 to 2023. This choice also helped reduce issues of data incompleteness due to cloud cover and tile edge effects, without being constrained by administrative boundaries.

3. Materials

3.1. VIIRS active fire data

We used VIIRS active fire product to identify fire occurrences. Specifically, the 375 m resolution VIIRS active fire data (VNP14IMGML) from the Suomi-NPP satellite was obtained via NASA's FIRMS (Fire Information for Resource Management System) archive (FIRMS, 2025). VIIRS provides global fire observations multiple times per day and offers enhanced nighttime fire detection compared to MODIS (Li et al. 2018). It employs dynamic contextual algorithms like MODIS but at finer spatial resolution, making it capable of detecting relatively smaller fire events. Each active fire record represents the center of a ~ 375 m pixel flagged as containing a fire or thermal anomaly (Schroeder et al., 2014). VIIRS's greater sensitivity at night and higher pixel density significantly improve the monitoring of fires in savanna environments (Justice et al., 2013; Li et al., 2018).

For this study, we filtered VIIRS active fires: low-confidence detections (potential false alarms from sun glint) were removed, and only fire-type events (excluding industrial heat sources like gas flares or volcanoes) with fire radiative power > 0 were retained. The final set of VIIRS fire points was used both to guide BA mapping and as independent indicators of fire timing and location.

3.2. Optical imagery: Harmonized Landsat-Sentinel-2

To map BA, we utilized the Harmonized Landsat and Sentinel-2 dataset (HLS) which fuses Landsat-8/9 OLI and Sentinel-2A/B MSI observations into a consistent 30 m, 2–3 day composite product. HLS provides surface reflectance data with atmospheric corrections, co-registration, and bandpass harmonization applied so that Landsat and Sentinel pixels are radiometrically comparable (Claverie et al., 2018). We accessed all available HLS images covering the study area from 2014 to 2023 (HLS v2.0; products L30 – Masek et al., 2021a and S30 – Masek et al., 2021b) using NASA's CMR-STAC API (EOSDIS, 2025). For each image date, we retrieved six spectral bands relevant to BA detection—Blue, Green, Red, near-infrared (NIR) broad and narrow bands, and two shortwave infrared (SWIR1, SWIR2) bands, along with the accompanying cloud mask (Fmask). These bands (detailed in Table 1) correspond to Landsat-OLI bands 2–7 and Sentinel-2 bands 2–4, 8 and 8A, as well as 11 and 12 (compare Tab. 1), covering visible blue (~0.49 μm) through SWIR (~2.2 μm) wavelengths. The high spectral and temporal resolution of HLS is crucial for accurately delineating burn scars shortly after fire events and distinguishing them from unburned vegetation.

3.3. Vegetation productivity: MODIS Gross/Net Primary productivity

To assess fire impacts on ecosystem productivity, we employed satellite-derived estimates of Gross Primary Productivity (GPP) and Net Primary Productivity (NPP) from the MODIS sensor. We obtained, from Google Earth Engine (GEE), the MOD17 Collection 6 datasets at 500 m resolution for the study period: the 8-day GPP product (MOD17A2H/MYD17A2H for Terra/Aqua) and the annual NPP product (MOD17A3H) (Running et al., 2004). GPP represents total carbon fixation by vegetation through photosynthesis, while NPP is the portion of GPP remaining after plant respiration losses, thus indicating net biomass accumulation. MOD17 uses a light-use efficiency model to estimate productivity, factoring in absorbed photosynthetically active radiation and stress scalars for temperature and moisture (Zhao et al., 2006). Although MODIS productivity data are relatively coarse, they provide consistent, validated measures of carbon flux suitable for regional assessments. For each year 2014–2023, we extracted the annual NPP and all 8-day GPP composites covering the region. These were used to calculate higher-temporal-resolution NPP (downscaled to 8-day, Section 4.2) to match fire occurrence timing.

The MODIS land cover product (MCD12Q1) was also used to stratify results by land use/land cover (LULC) type, classifying each pixel (500 m) into categories such as savanna, forest, cropland, etc., based on the IGBP scheme (Friedl and Sulla-Menashe, 2019). This dataset was selected because of its consistent annual coverage (2001 to present), aligning with our study period. Although higher-resolution products like ESA WorldCover (10 m) offer more detailed classifications, they typically suffer from inconsistent annual updates entire study area. The MODIS product was chosen for its reliable temporal coverage and global extent, making it ideal for our long-term analysis of land cover change and post-fire recovery in West Africa.

3.4. Other satellite data

We included additional environmental variables known to influence fire severity and recovery (Wulder et al., 2021; Shang et al., 2022). These factors were selected based on their documented influence on fire behaviour, severity, and ecosystem recovery. Specifically, moisture availability is critical because it determines plant regrowth potential and fire intensity. To capture moisture variability, we derived the

Table 1
Harmonized Landsat and Sentinel-2 (HLS) spectral bands used for burned area mapping, with approximate Landsat OLI and Sentinel-2 MSI equivalents and central wavelengths. (Abbreviations: NIR – near-infrared; SWIR – shortwave infrared; B – band.).

Band name	OLI band number	MSI band number	HLS bands codename Landsat-8	HLS band code name Sentinel-2	Wavelength (micrometers)
Blue	2	2	B02	B02	0.45 - 0.51*
Green	3	3	B03	B03	0.53 - 0.59*
Red	4	4	B04	B04	0.64 - 0.67*
NIR Broad	–	8	–	B08	0.78 – 0.88**
NIR Narrow	5	8A	B05	B8A	0.85 - 0.88*
SWIR 1	6	11	B06	B11	1.57 - 1.65*
SWIR 2	7	12	B07	B12	2.11 - 2.29*

* from OLI specifications; ** from MSI specifications.

Normalized Difference Moisture Index (NDMI) from the HLS data. NDMI is calculated as (NIR – SWIR) / (NIR + SWIR), using reflectance in the narrow NIR band (~0.86 μ m) and SWIR1 (~1.6 μ m). NDMI is sensitive to water content in vegetation and soil; higher NDMI values indicate wetter conditions. We generated NDMI time series for the study area at 30 m resolution, concurrent with pre- and post-fire image composites.

Temperature, land surface temperature (LST) influence fire behaviour, with higher temperatures typically resulting in more intense fires. In parallel, precipitation and air temperature provide vital information on climate anomalies, such as droughts, which affect fuel availability and recovery post-fire. Collectively, these variables capture both the immediate effects of fire (e.g., intensity, duration) and long-term recovery potential (e.g., regrowth, moisture availability).

LST was derived from Landsat-8 thermal infrared data using the single-channel algorithm by Ermida et al. (2020) within GEE. The retrieved LST data (in °C) at 30 m resolution were aggregated to monthly means to represent background temperature conditions during the dry season. Climate variables, including total precipitation and mean 2 m air temperature from ERA5 reanalysis (Hersbach et al., 2020), were extracted for each month at a spatial resolution of approximately 11 km (0.1°). Despite the relatively coarse resolution, these climate datasets offer crucial contextual insights into rainfall deficits and heat anomalies that could influence both fire behaviour and vegetation regrowth.

All spatial datasets were co-registered and resampled to a common 30 m grid that spans the entire study area, aligned with the HLS pixel grid, ensuring consistency and enabling the integration of the datasets for analysis.

To incorporate edaphic factors into the post-fire recovery analysis, we integrated standardized global soil data from SoilGrids (Batjes and van Oostrum, 2023), provided by ISRIC. The dataset delivers gridded soil estimates at 250 m resolution, suitable for regional-level analyses, although higher resolution data would offer more precise insights. Variables were extracted for the 0–5 cm depth interval, which corresponds to the surface processes influencing fire effects and vegetation regrowth.

The following soil parameters were included in the analysis:

- Soil texture class: derived from the clay, silt, and sand fractions using USDA thresholds. Each pixel was assigned to one of 12 texture classes, enabling the modelling of soil physical properties.
- Soil organic carbon (SOC): reflecting topsoil fertility, SOC plays a key role in post-fire vegetation productivity by supporting regrowth.
- Nitrogen content: representing the total nitrogen in the soil, this serves as a proxy for nutrient availability, critical for plant recovery.
- Water retention at 10 kPa and 1500 kPa: representing plant-available water and wilting point moisture, respectively, these values are essential for understanding water limitations during post-fire recovery.
- Soil classification: classifying the soils according to the World Reference Base for Soil Resources (WRB) provides broader insights into functional soil differences and their role in fire recovery.

In addition to other environmental variables, we used the MODIS MCD12Q1 land cover product, which provides annual global land use/land cover classifications at a 500 m resolution. This dataset was selected because of its consistent annual coverage (2001 to present), aligning with our study period. Although higher-resolution datasets like Landsat or Sentinel-2 offer more detailed classifications, they typically suffer from inconsistent annual updates and missing data for our entire study area. The MODIS product was chosen for its reliable temporal coverage and global extent, making it ideal for our long-term analysis of land cover change and post-fire recovery in West Africa.

To ensure spatial consistency, all datasets were resampled to match the 30 m grid of the HLS imagery. MODIS-based variables (GPP, NPP, and land cover) and climate variables were processed in GEE, which performs automatic internal resampling when datasets are reprojected or exported at resolutions finer than their native scale (Google Developers, 2024). Continuous data were resampled using bilinear interpolation and categorical data with nearest-neighbour resampling. SoilGrids data (250 m) were resampled in R using the terra package (Hijmans, 2025), with bilinear interpolation for continuous attributes (e.g., nitrogen, water retention) and nearest-neighbour for categorical layers. All resampling operations used the HLS extent and resolution as reference to preserve spatial alignment across layers.

4. Methods

The workflow of this study has four major steps (Fig. 2). An important distinction to highlight is the definition of the fire season and the study period. In the study area, the fire season aligns with the dry season, which typically begins in November and extends through April of the following year. Consequently, the fire season in this study was defined similarly. For instance, the 2019 fire season spans from November 2018 to April 2019. This approach was consistently applied for fire seasons from 2014 to 2023.

BA mapping: The first step involves generating monthly BA datasets at a 30-meter spatial resolution using HLS data combined with VIIRS active fire.
Estimating productivity loss: The second step estimates the loss in NPP and GPP caused by fires. Since these productivity datasets are available at a coarser resolution (500 m), they were resampled to align with the BA data's 30 m resolution. This resampling ensures consistency and facilitates integration in subsequent analyses.
Post-fire vegetation recovery: The third step evaluates vegetation recovery trajectories at both monthly and annual time scales. This analysis examines how vegetation recovers over time following fire disturbances, providing insights into ecosystem resilience.
Identifying drivers of recovery: The final step assesses potential factors influencing recovery rates. This includes evaluating variables such as fire frequency, land cover, climatic variables, soil properties and moisture to understand their roles in shaping post-fire recovery dynamics.

All statistical analyses were conducted in R and significance was assessed at the 95 % confidence level unless otherwise noted.

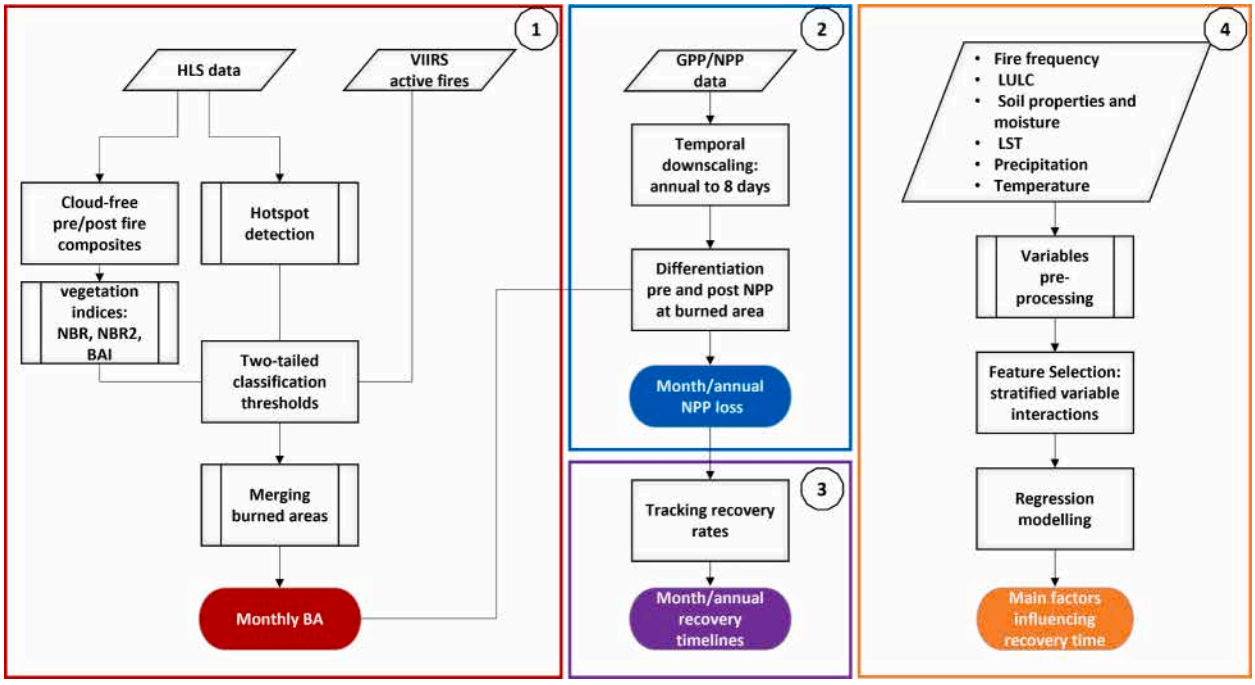

Fig. 2. Conceptual framework illustrating the workflow for understanding fire-driven Net Primary Productivity (NPP) loss, post-fire recovery trajectories, and their potential influencing factors.

4.1. Burned area mapping

Our BA mapping approach (Fig. 2, sub-section 1) combined multi-spectral change detection with active fire information to delineate burned patches at 30 m spatial resolution. The procedure was implemented in monthly time steps.

Pre- and post-fire composites.

For each month with available HLS imagery, we constructed a pair of cloud-free composite images representing the pre-fire and post-fire conditions. The month of interest (e.g., January 2019) is the target month for BA detection. The pre-fire composite covers approximately one month before the fire (from the start of the preceding month up to the day before the target month begins), and the post-fire composite covers about one month after the fire (from the start of the target month through the end of the following month). To create these composites, we used the maximum and minimum value compositing approach, respectively, for the pre-fire and post-fire periods. For the pre-fire composite, the maximum values of each pixel across all available imagery within the one-month period were selected, representing the "healthiest" state of the landscape with minimal cloud cover and disturbances. For the post-fire composite, the minimum values of each pixel were chosen, capturing the most severely affected areas by fire, as this corresponds to the lowest spectral reflectance after the burn. This approach accentuates the spectral differences caused by burning, highlighting areas with substantial loss of vegetation cover.

Cloud and land cover masking.

We applied rigorous masking to remove non-valid pixels. First, we utilized the HLS Fmask layer to exclude clouds and cloud shadows (Zhu and Woodcock, 2014). Any pixel flagged as cloud/shadow in any image contributing to the composites was masked out. We then applied additional spectral filters: pixels with abnormal blue reflectance (<0.15) or very high SWIR2 reflectance (>0.5 %) consistent with clouds were also masked (Roteta et al., 2021), complementing Fmask step. Open water and urban areas were masked using the ESA WorldCover 2020 land cover map (Zanaga et al., 2021) to avoid confusion with dark water or built surfaces that have similar spectral properties as BA.

Spectral indices for burn detection

We calculated three spectral indices known to be sensitive to burning: the Normalized Burn Ratio (NBR), NBR2, and the Burned Area Index (BAI). The formulas and spectral bands used for these indices are presented in Table 2. The NBR and its variant NBR2, designed to assess burn severity, exploit changes in reflectance within the near-infrared and mid-infrared regions (Veraverbeke et al., 2011; Atak and Tonyaloğlu, 2020; Rossetti et al., 2022). The NBR index typically ranges from −1 to 1, where values close to 1 represent healthy vegetation, negative values indicate severe burn (more negative values reflecting more intense burns), and values near zero often correspond to BA. NBR2 is similar but uses a broader mid-infrared band range, providing an enhanced sensitivity to low-severity burns (NBR2 ranges from −0.2 to 0.6, with lower values indicating higher burn severity) (Storey et al., 2016; van Gerrevink and Veraverbeke, 2021).

Moreover, BAI provides critical insights into post-fire vegetation recovery and resilience, making it indispensable for ecological evaluations (Marcos et al., 2018; Liu et al., 2021). BAI values range from 0 (indicating no burn or no vegetation) to higher positive values, with higher BAI values representing more extensive burning and lower values indicating less burn impact. For each index, the pre-fire, post-fire, and difference values were calculated, which were used both in image classification and in the sampling process to distinguish burned and

Table 2
Spectral indices used for burned area mapping and their formulae, derived from Harmonized Landsat and Sentinel-2 (HLS) data. *RED* = reflectance in the red band, NIR = reflectance in the near-infrared band; SWIR = reflectance in the shortwave infrared band.

Spectral indices		Equation	Reference
Acronym	Full name		
BAI	Burned Area Index	$\frac{1}{(0.1-RED)^2+(0.6-NIR)^2}$	Chuvieco et al., 2002
NBR	Normalized Burn Ratio	$\frac{NIR-SWIR2}{NIR+SWIR2}$	Key and Benson, 1999
NBR2	Normalized Burn Ratio 2	$\frac{SWIR1-SWIR2}{SWIR2+SWIR2}$	Key and Benson, 2006

unburned candidate pixels.

Active fire integration (Hotspots).

We incorporated both the VIIRS active fire data and Murphy et al.'s (2016) hotspot algorithm to improve our BA search. The VIIRS active fire points were buffered by 375 m (the nominal VIIRS pixel size) to define regions where fire activity was likely, and these buffers were merged with hotspots derived from HLS imagery based on Murphy et al. (2016).

In this method, we identified "hot pixels" in the HLS imagery by detecting reflectance anomalies that indicate recent burning. Specifically, Murphy et al. (2016) use two key variables, α (alpha) and β (beta), to flag potential fire pixels:

- α: represents pixels where NIR reflectance is anomalously low (a signature of burnt or stressed vegetation).
- β: represents pixels where SWIR reflectance is anomalously high, suggesting the presence of fire-affected surfaces.

Each pixel's NIR and SWIR reflectance values were compared against predefined threshold values based on these anomalies. If the reflectance values fell outside the expected range for healthy vegetation, the pixel was flagged as a potential fire hotspot.

To further refine our analysis, we combined the VIIRS fire points (with their 375 m buffer) and Murphy's HLS-derived hotspots to identify regions with confirmed fire activity. A minimum cluster size of 100 pixels (~9 ha) was required for burn delineation, ensuring that small or isolated fire signals were not misclassified as burns. If no fire signals were detected in a given area, it was assumed that no burn occurred for that month, reducing false positives. This approach ensures that only areas with evidence of fire activity from both the active fire data and the HLS hotspot algorithm are considered, improving the precision of our BA detection.

Two-tailed thresholding.

We employed a two-tailed threshold approach on the spectral index distributions to classify burned vs. unburned pixels. Specifically, for each index (e.g., NBR), we calculated percentile-based thresholds for both fire-affected areas and non-fire areas. This was done for both pre-fire and post-fire conditions.

To do this, we:

- For fire-affected areas: identified the typical range of index values by calculating the percentiles (e.g., 5th, 95th) for the pre-fire and post-fire indices in regions that had been impacted by fire.
- For non-fire areas (control areas): calculated their own pre/post-fire percentiles to prevent other non-fire-related changes, like phenology shifts, from being misclassified as fire.

A pixel was labelled as burned if its pre-fire index value fell below the calculated fire threshold, and its post-fire value was sufficiently lower, indicating a significant decrease in vegetation health. DeltaNBR (ΔNBR) refers to the difference in NBR before and after the fire, and we used this to quantify the magnitude of the burn. If the pixel had a sufficient ΔNBR (a large decrease), it was classified as burned. This approach was applied separately for the NBR, NBR2, and BAI indices. This method is particularly effective in heterogeneous landscapes, such as in West Africa (Laris, 2005), where vegetation and land cover variability pose challenges to traditional BA mapping techniques. For the period of interest (month), regions affected by fire are those overlaid by identified hotspots from the previous sub-section.

Burn scar identification

The preliminary burn classification from each index was combined. We used a majority consensus rule requiring at least two out of the three indices to agree on a pixel being burned. This reduces false positives that might arise if a single index is noisy or affected by non-fire factors. The resulting burned pixels were aggregated into contiguous patches, and very small or linear features (likely false detections or fire lines) were eliminated. Finally, we visually inspected the monthly BA maps against original imagery for quality control, and then mosaicked all months to obtain the full BA dataset for 2014–2023.

On a monthly basis, pixels were categorized into one of the following four groups based on their fire frequency during the 2014–2023 fire seasons:

- rarely burned: burned fewer than 7 times in the study period (<7).
- occasionally burned: burned between 7 and 12 times (7–12).
- moderately burned: burned between 13 and 18 times (13–18).
- frequently burned: burned more than 18 times (>18).

This categorization enabled the stratification of areas by burn intensity and recurrence over the study period, providing a proxy for burn severity. This information was also used in the drivers of recovery time assessment.

Burned area performance.

Our BA mapping algorithm was validated and compared with existing products. We performed an accuracy assessment using reference fire perimeters from the Burned Area Reference Database (BARD). Specifically, we used the FireCCI Africa 2019 dataset (Stroppiana et al., 2022) derived from Sentinel-2 for five sample tiles (15 × 15 km each) in West Africa. These reference polygons for burned/unburned areas in 2019 were compared to our monthly BA outputs for the corresponding locations and period. Standard metrics including omission and commission errors, and the Dice coefficient, were computed to quantify agreement. Additionally, we conducted an intercomparison by overlaying our BA maps with several widely-used BA products that cover the study region: FireCCI51 (MODIS 250 m, Chuvieco et al., 2018), FireCCI SFD20 (Sentinel-2 20 m, Chuvieco et al., 2022), FireCCIS310 (Sentinel-3, 300 m, Lizundia-Loiola et al., 2022), VIIRS-BA (VIIRS 375 m, prototype product by Ouattara et al., 2024), and MCD64A1 Collection 6 (MODIS 500 m, Giglio et al., 2018). We compared spatial patterns of burn detection for selected subsets (Comoé National Park and Dano) to illustrate differences, especially in capturing small fires. These intercomparisons were qualitative (not a formal validation) and only meant to highlight relative strengths of our approach.

4.2. Net primary productivity loss calculation

To quantify the loss of productivity due to fire, we calculated the difference between expected NPP in the absence of fire and the observed NPP after fire. A challenge is that MODIS NPP is annual; to attribute NPP loss to specific fire events and seasons, we downscaled NPP in time using the higher-frequency GPP data. We employed a proportional downscaling approach: for each pixel and year, the fraction of annual GPP occurring in each 8-day period was used to partition the annual NPP into 8-day increments, as represented in Equation (1):

$$\mathrm{NPP}_{8d} = \left(\frac{GPP_{8d}}{GPP_{y}}\right) \times \mathrm{NPP}_{y} \quad (1)$$

Where: NPP_{8d} represents the downscaled yearly NPP to an 8-day composite; GPP_{8d} refers to GPP data already available at an 8-day composite; GPP_{yr} is the sum of GPP_{8d} for a given year (y) and NPP_{y} is the annual NPP composite data available at the yearly scale

We then aggregated these into monthly NPP totals and also into fire-season NPP (summing from November through April for each fire season year) to match our fire analysis periods.

For every pixel that burned, we defined the pre-fire NPP as the NPP in the last full month prior to burning (for monthly analysis) or the year preceding the fire year (for annual analysis). The post-fire NPP was taken as the NPP measured during or after the fire event. The NPP loss due to a fire was then computed as:

- Monthly scale: $\Delta NPP_m = NPP_{m(pre\text{-}fire)} - NPP_{m(post\text{-}fire)}$ in the same fire season. For example, if a fire occurred in December, we compare October NPP (pre-fire baseline for that pixel) to December or subsequent months' NPP.
- Annual scale: $\Delta NPP_y = NPP_{y(pre\text{-}fire\ year)} - NPP_{y(fire\ year)}$. If an area burned in the 2018–2019 fire season, we compare total NPP of 2018 to that of 2019 in that pixel.

We masked these calculations to only fire-affected pixels using our BA maps: ΔNPP was computed only within the BA, effectively attributing productivity loss to fire-disturbed zones. Summing ΔNPP over all burned pixels gives the total carbon productivity lost to fires in the region for a given period. We normalized the ΔNPP by dividing the total NPP loss by the area of the burned pixels (i.e., total BA in hectares). This gives the NPP loss density, expressed as Mg C ha^{-1} burned. This approach allows comparison of fire impact severity across regions and land cover types.

We stratified the NPP loss analysis by land cover category (MODIS MCD12Q1) to see how different ecosystems respond to fire. We additionally examined trends in annual NPP loss over 2014–2023 using the Mann-Kendall non-parametric test ($\alpha = 0.05$), via the Kendall package in R software (McLeod, 2011), to detect any significant increase or decrease in fire-related carbon loss. Finally, we computed the ratio of NPP loss to BA for each year and location, as mentioned, to identify hotspots of disproportionately high or low impact areas where small burns cause large productivity drops or vice versa.

4.3. Post-fire vegetation recovery analysis

We assessed vegetation recovery times after fire at two temporal scales: monthly (short-term) and multi-year (long-term). Recovery was defined in terms of NPP returning to baseline levels. For monthly recovery, we defined the pre-fire baseline as the October NPP – the last full month before the fire season. While this captures peak productivity in many forested zones, in some grassland systems September might represent the actual productivity maximum. For annual recovery, the baseline was the NPP of the year 2014 (the first year of our analysis), under the assumption that areas unburned since 2014 had stable or increasing productivity up to a fire event.

For each burned pixel, we tracked the time series of NPP after the fire and identified the first time it equalled or exceeded the pre-fire baseline. The time to recovery was counted in months for the short-term analysis (with a maximum window of 12 months beyond the fire) and in years for the long-term analysis (up to 9 years beyond the fire, given our 2014–2023 data range). If NPP never recovered to baseline within the period of record, the pixel was labelled as "unrecovered". Using this approach, we generated maps of recovery time, effectively measuring ecosystem recovery patterns both spatially and temporally.

We then classified recovery time into categories to facilitate interpretation.

For monthly recovery: *Immediate* (within 1 month), *Short-term* (2–3 months), *Medium-term* (4–5 months), *Long-term* (6–7 months), and *Not recovered* in 7 months or more.

For annual recovery: *Fast* (1 year), *Moderate* (2–3 years), *Gradual* (4–5 years), *Delayed* (6–7 years), *Very Delayed* (8–9 years), or *Not recovered* by 2023. These thresholds were chosen based on natural breaks in the data distribution and ecological relevance (e.g., recovery within one growing season vs. multiple years).

Furthermore, to understand differences among ecosystems, we stratified recovery outcomes by LULC type (savannas, forests, grasslands, croplands). This reveals, for example, if forests systematically take longer to recover than grasslands, or if agricultural areas show unique patterns due to human intervention (like replanting). We also examined the spatial clustering of slow vs. fast recovery areas to see if certain regions (e.g., particular parks or climate zones) exhibit notable delayed regrowth.

4.4. Drivers of recovery time

We investigated which environmental and biophysical factors best explain the variability in post-fire vegetation recovery time across the burned pixels. For this, we constructed a spatially explicit dataset of recovery outcomes and potential predictor variables at 30 m resolution, matching the resolution of the BA and vegetation data. Recovery time (in years) was used as the response variable, derived from time-series NPP analysis as previously described.

The predictor variables included:

- fire regime: burn frequency (number of times a pixel burned between 2014 and 2023)
- land cover: MODIS LULC classification
- climate: mean annual precipitation and temperature (from ERA5)
- vegetation moisture and aridity: mean dry-season NDMI (from HLS) and mean dry-season LST (from Landsat)
- soil properties: soil texture class, nitrogen content, Soil organic matter water retention at 10 kPa and 1500 kPa, and Soil Classification.

Vegetation characteristics were represented via land cover categories from MODIS MCD12Q1. While this provides broad structural types (forest, grassland etc.), it does not capture species composition or fine-scale traits (e.g., resprouting ability, leaf area index), which likely also influence recovery patterns but were not explicitly assessed.

To allow the model to capture non-linear effects and interactions, we created pairwise interaction terms between continuous variables (e.g., NDMI × temperature) and between continuous and categorical variables (e.g., NDMI × land cover class). In total, over 100 features were generated, including original predictors and interaction terms.

We employed a machine learning approach using the H2O AutoML framework (within R software with the package H2O, Fryda et al., 2024) to build predictive models of recovery time. AutoML trained and evaluated multiple algorithms including gradient boosting machines (GBM), random forest, extreme gradient boosting (XGBoost), neural networks, and generalized linear models on our dataset. We reserved 30 % of the data for validation, training models on the remaining 70 %. AutoML also performed automated feature selection to drop irrelevant predictors, and iteratively tuned hyperparameters within a given time/resource limit (we allowed up to 10 models per algorithm). Model performance was ranked by the lowest mean residual deviance on the validation set. The top-performing model was chosen for interpretation.

From the best model, we extracted variable importance metrics to identify which factors contributed most to explaining recovery time variability. Additionally, we explored key interactions and partial dependence effects to interpret the influence of specific environmental gradients (e.g., soil water retention vs. NDMI) on recovery trajectories. This integrative approach helps disentangle how both aboveground (e.g., climate, fire regime) and belowground (e.g., soil fertility, water holding capacity) factors modulate vegetation recovery dynamics in West African savannas. We did not include SHAP or partial dependence plots analyses to avoid dispersing focus; permutation importance suffices for our objectives and aligns with common practice in eco-climate studies (Bradter et al., 2022; Thuiller, 2024).

5. Results

5.1. Burned area dynamics

Spatio-temporal patterns.

Annual fire activity in the study area is strongly seasonal. Fig. 3 shows the intra-annual distribution of BA. Early dry season burns (November–December) dominate, followed by the middle dry season (January–February), while the late dry season (March–April) contributes the least. December is consistently the peak month, accounting for

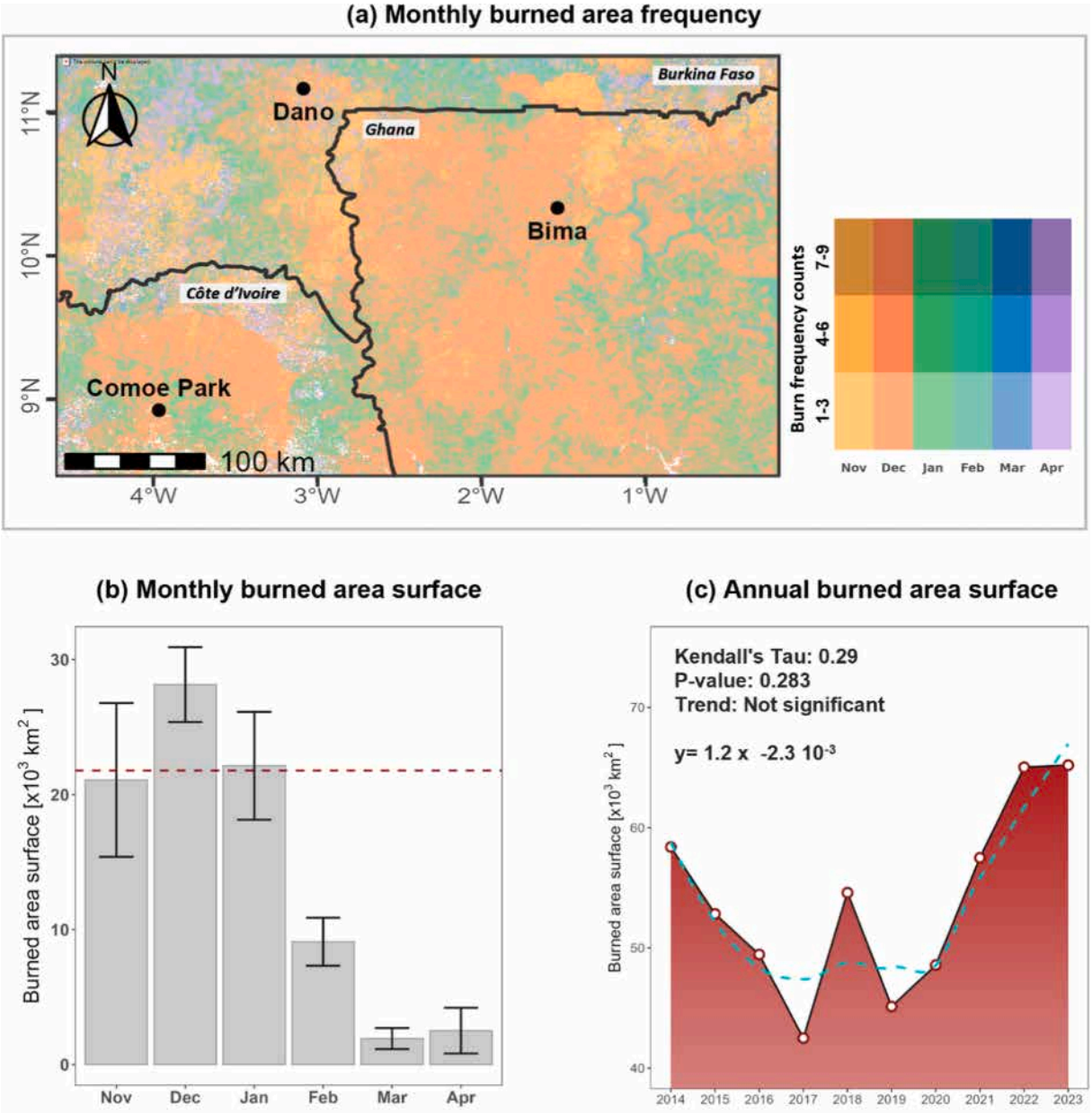

Fig. 3. Burned area seasonality and trends (2014–2023). (a) Spatial distribution of mean monthly burned area frequency (number of years in which a given pixel burned in each month, visualized as intensity per month). (b) Total area burned per month, averaged over the decade, showing the dominant contribution of Nov–Dec. (c) Annual burned area time series with loess regression (dashed line) and Mann-Kendall trend result. December is the peak month each year, and interannual variability is evident, with a mild increasing tendency that is not statistically significant.

about one-third of the total annual BA on average. Summed over 2014–2023, November through January contributed > 84 % of all BA each year. In absolute terms, the region experienced on average 22 × 10^3 km^2 of area burned per year, with year-to-year variation (std ~ 8 × 10^3 km^2). Spatially, burns were widespread across the savanna portions of all three countries, but certain hotspots emerged. Fire season typically onset in November, rapidly peaked by December, and then declined. A minor resurgence in April was observed in a few years, likely associated with late dry-season agricultural fires or localized droughts extending the fire window.

Inter-annual trends (Fig. 3c) indicate a slight upward trend in BA over the decade, but this trend is not statistically significant. The non-parametric Mann-Kendall test yielded a tau corresponding to + 0.29 % per year ($p > 0.05$), suggesting no clear increase or decrease. A linear fit illustrates that BA was relatively low in the mid-2010 s (minimum around 2017 coinciding with a notably wet year that reduced fires), followed by a rise post-2018. By 2023, BA slightly exceeded the 2014 level, reflecting a possible resurgence of fire activity in recent years. This could be related to climate variability or socio-economic factors (e.g., shifts in land management).

Burned area frequency categories.

We classified pixels based on how frequently they experienced fire during the 2014–2023 fire seasons (Fig. 4). The majority (~60 %) of the study area fell into the "rarely burned" category (burned fewer than 7 times during the study period). These rarely BA include most of the agricultural zones in southern Burkina Faso and northern Côte d'Ivoire, as well as parts of the northernmost sparse savannas.

About 34 % of the area was "occasionally burned" (burned 7–12 times), predominantly in northern Ghana and scattered patches elsewhere. The "moderately burned" class (13–18 times) covered around 5 % of the landscape and tended to concentrate in ecologically important zones such as Comoé National Park and the Bima region, as well as some

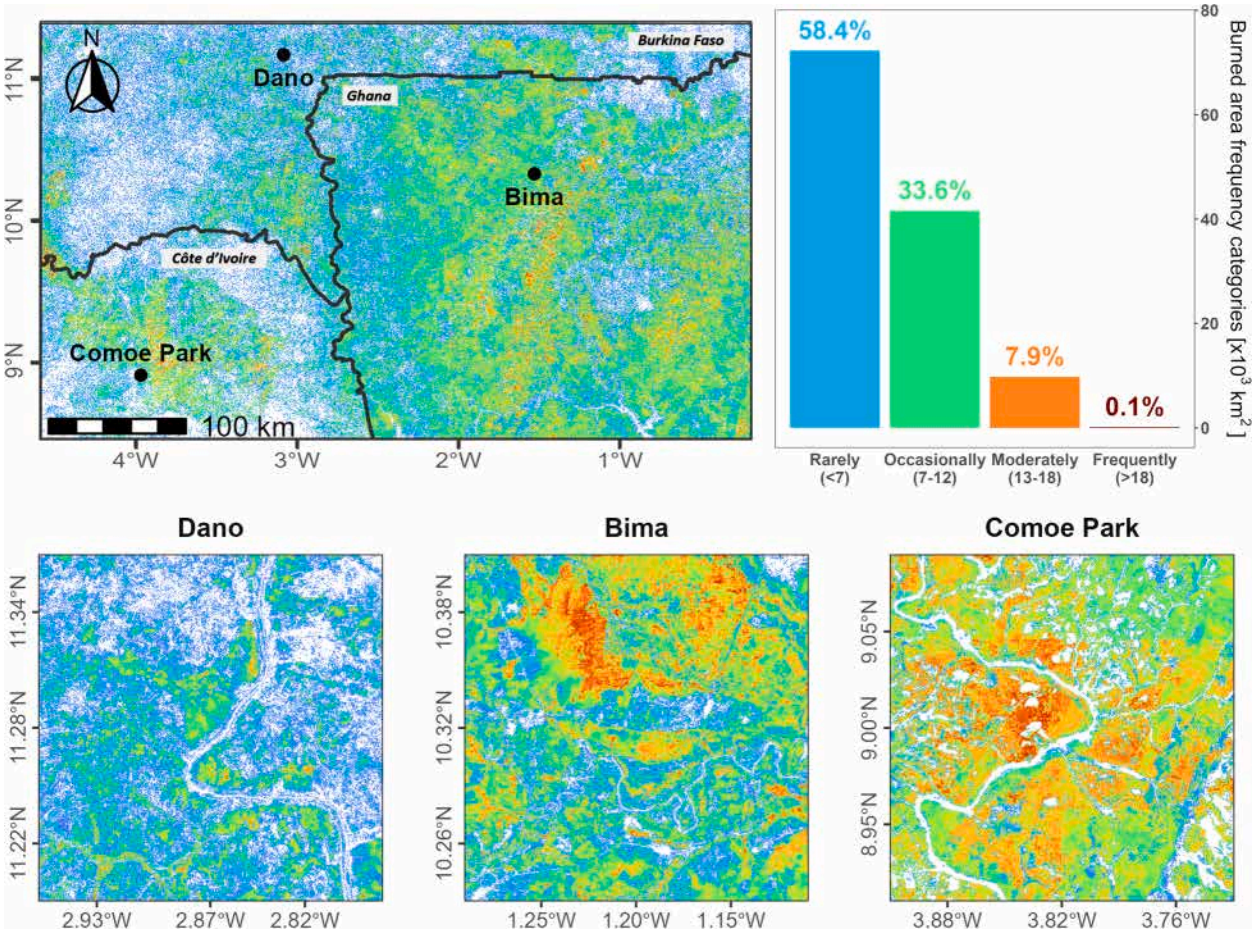

Fig. 4. Fire frequency map (2014–2023) categorizing areas by burn frequency (counts are per month during the 2014–2023 fire seasons): rarely burned (<7), occasionally burned (7–12), moderately burned (13–18), frequently burned (>18). Insets highlight examples from Dano, Bima, and Comoé National Park, showcasing landscapes with moderate-to-high fire recurrence.

parts of Burkina Faso's savannas. These areas experience fire roughly every other year on average and are often described as having a natural fire regime. However, in protected areas like Comoé or PONASI, these fire patterns are largely influenced by human activity, particularly hunting fires and traditional land use (Laris, 2011).

Lastly, "frequently burned" areas (burned more than 18 times) made up less than 1 % of the area. There was no large contiguous zone of frequent burns; instead, these were small pockets, often near Bima (Ghana) and at the edges of Comoé National Park. While these zones appear naturally fire-prone, they are typically maintained by repeated human burning—especially for early dry-season grass clearing in short-grass savannas or bowe types (Laris, 2011). The low proportion of this class suggests that, while fire is widespread, very frequent burning is limited to specific anthropogenically maintained sites, such as

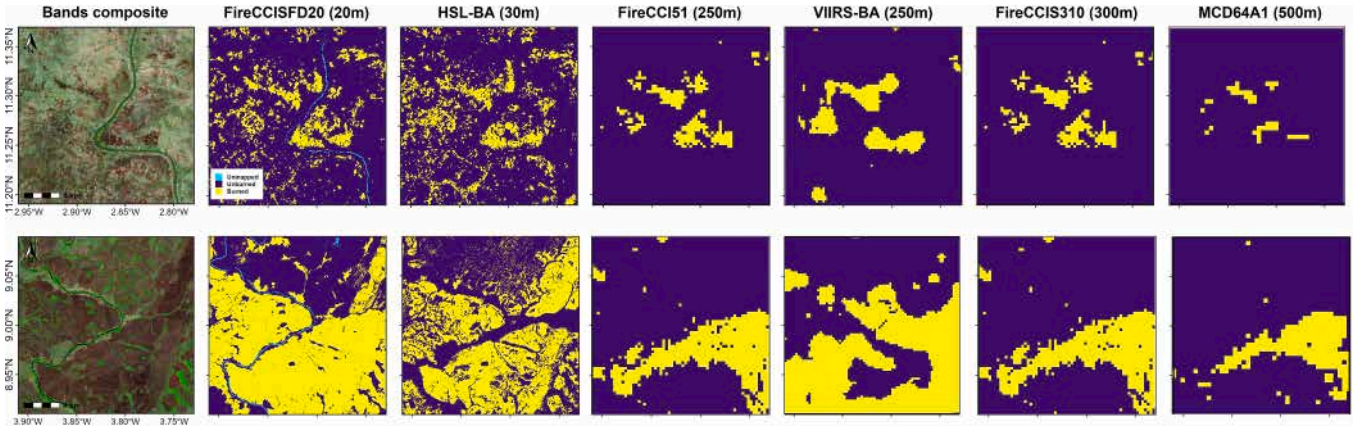

Fig. 5. Burned area comparison in two example areas (upper row: Dano, Burkina Faso; lower row: Comoé National Park, Côte d'Ivoire, January 2019). Each panel shows a true-color image with burn scars, and the burn classification from: This study (HLS-BA, 30 m), FireCCISFD20 (Sentinel-2, 20 m; Chuvieco et al., 2022), FireCCI51 (MODIS, 250 m; Chuvieco et al., 2018), VIIRS-BA prototype (375 m; Ouattara et al., 2024), FireCCI310 (300 m; Lizundia-Loiola et al., 2022), MCD64A1 (MODIS, 500 m; Giglio et al., 2018).

rangelands and annually burned fields.

Burned area mapping accuracy.

Our BA product was evaluated against high-resolution reference data and other BA datasets. The comparison with BARD fire perimeters for 2019 showed good agreement: our monthly mapping correctly identified 89 % of the reference burned polygons (omission error ~ 11 %) and had a commission error of ~ 15 %. Many of the omitted fires were extremely small (<0.5 ha) or occurred under heavy cloud cover, highlighting the challenges of full detection. The overall accuracy against BARD was 95 %, indicating reliable performance in delineating burned vs. unburned areas at 30 m.

Intercomparison with other products.

Fig. 5 illustrates how our BA map compares to several existing products in two example subsets (10 × 10 km) in Dano (Burkina Faso) and Comoé National Park. The high-resolution FireCCISFD20 (Sentinel-2, 20 m) is the closest to ours in resolution and showed very similar burn patterns, often detecting the same small burn scars. MODIS-based products (FireCCI51 at 250 m, MCD64A1 at 500 m) tended to miss many of the finer burns, only capturing the larger fire-affected areas as larger, more continuous patches. Our product and FireCCISFD20 captured intricate shapes of burned patches—long narrow burns along riverbanks, small circular farm burns—those coarser datasets either generalized or omitted. For instance, in Comoé National Park subset, a series of small burns under 5 ha are clearly visible in our 30 m map and the 20 m Sentinel-based map, whereas the 250 m and 500 m maps either show nothing or a single large burned polygon merging them. This demonstrates the added value of higher spatial resolution for burn mapping in these fragmented savanna-forest landscapes. The VIIRS-BA (375 m) product performed intermediate—detecting some, but not all, small fires. Overall, the results emphasize that fine-scale burns, which can constitute a significant portion of total fire events in West Africa, are much better accounted for in our HLS-based dataset. Such detail is crucial for ecological assessments (understanding patchy fire effects on vegetation) and management strategies (like planning fire breaks or controlled burns), especially in areas where fire sizes are inherently small due to human landscape fragmentation or fuel distribution.

5.2. Ecosystem productivity reduction

Spatio-temporal dynamics of net primary productivity loss.

In our analysis, we explicitly distinguish seasonal (monthly) versus annual fire-induced NPP losses. In the results, we refer to seasonal NPP loss as the productivity reduction occurring in a given month of the dry-fire season (Fig. 6a), whereas annual NPP loss is the total yearly productivity deficit from all fires (Fig. 6b). Fig. 6a shows the average monthly NPP loss during the fire season. December and January, which have the most extensive burning, showed the highest NPP loss, each losing on average ~ 3.8–12.6 × 10^{-2} Mg C ha^{-1} (as NPP) per month. Combined, December–January accounted for the bulk of the fire-

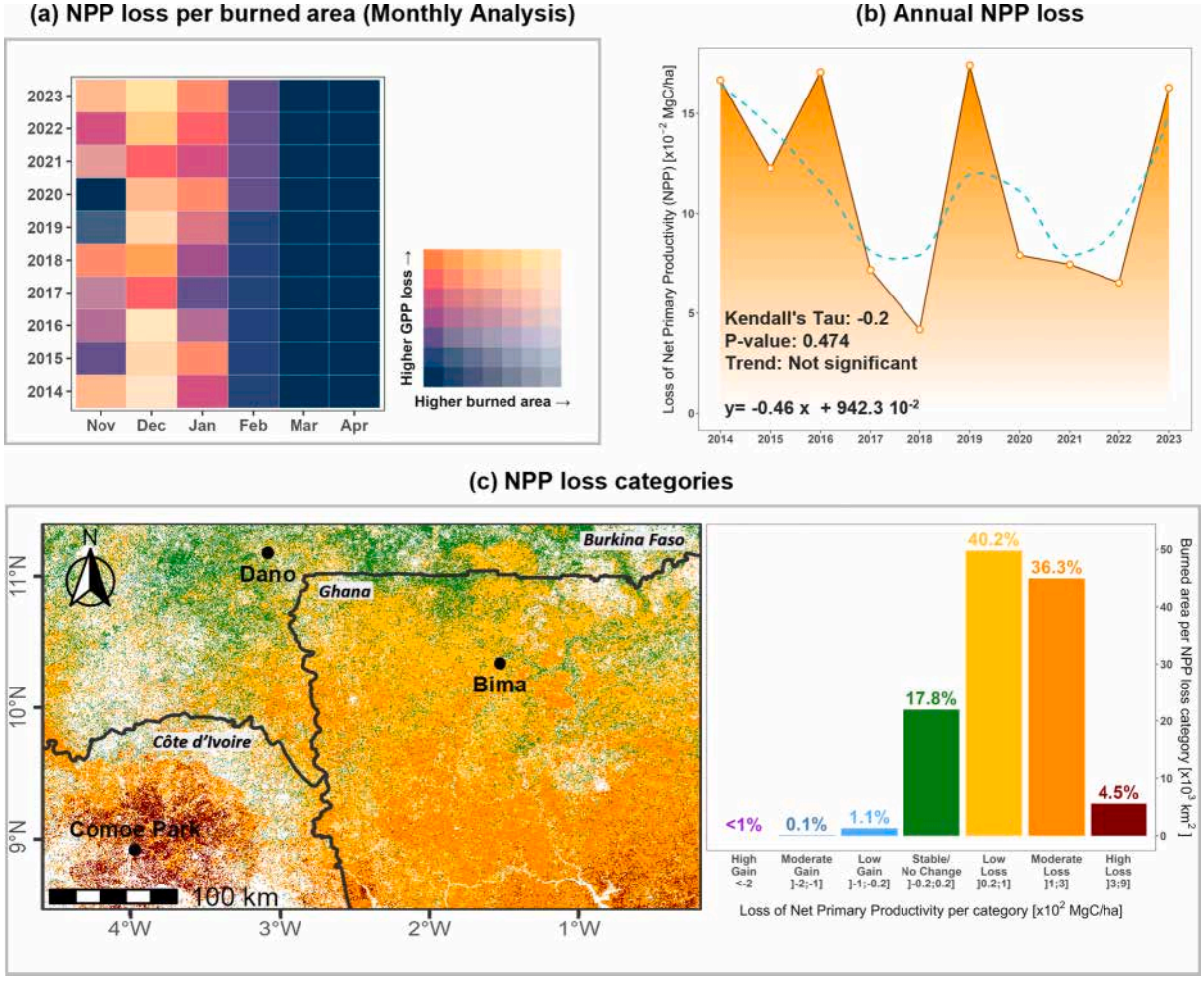

Fig. 6. Fire-induced Net Primary Productivity (NPP) loss. (a) Mean monthly NPP loss during the fire season (Nov–Apr), highlighting peak losses in Dec–Jan. (b) Interannual variation of total NPP loss with no significant trend over 2014–2023. (c) Spatial distribution of cumulative NPP loss (Mg C ha^{-1}) attributable to fires, 2014–2023. Northern savannas show minimal loss or slight gains (green/blue), central areas moderate loss (yellow), and southern areas and forest patches high loss (red).

induced productivity deficit (~1.6 Mg C ha^{-1}). By contrast, March and April, when fires are fewer and smaller, showed a decrease in NPP, with average monthly values of ~ 1.6 × 10^{-2} Mg C ha^{-1} for March and ~ 1.3 × 10^{-2} Mg C ha^{-1} for April, indicating an increase in productivity in those months due to lower fire intensity and biomass reduction. This suggests that the timing of fires has a clear relationship with carbon impact: early dry-season fires remove productive vegetation that would have otherwise fixed carbon through the dry season, whereas late-season fires tend to find less biomass as many annual grasses have already senesced, resulting in smaller carbon flux perturbations. Over the 10-year period, December was consistently the peak month for NPP loss each year.

At the annual scale (Fig. 6b), total NPP loss to fires in the study area averaged about 11 × 10^{-2} Mg C ha^{-1} per year, which represents the carbon that would have been stored if fires had not occurred. Year-to-year variation in NPP loss mirrored the BA trends. The lowest fire impact was in 2018, which corresponded to 2017′s low fire activity; that year's NPP loss was minimal, reflecting relatively undisturbed vegetation growth. There were noticeable oscillations: for example, NPP loss dropped in 2016–2018 and then rose after 2019, paralleling the BA increase. However, the Mann-Kendall trend test on annual NPP loss showed no significant trend ($p > 0.1$), indicating that despite

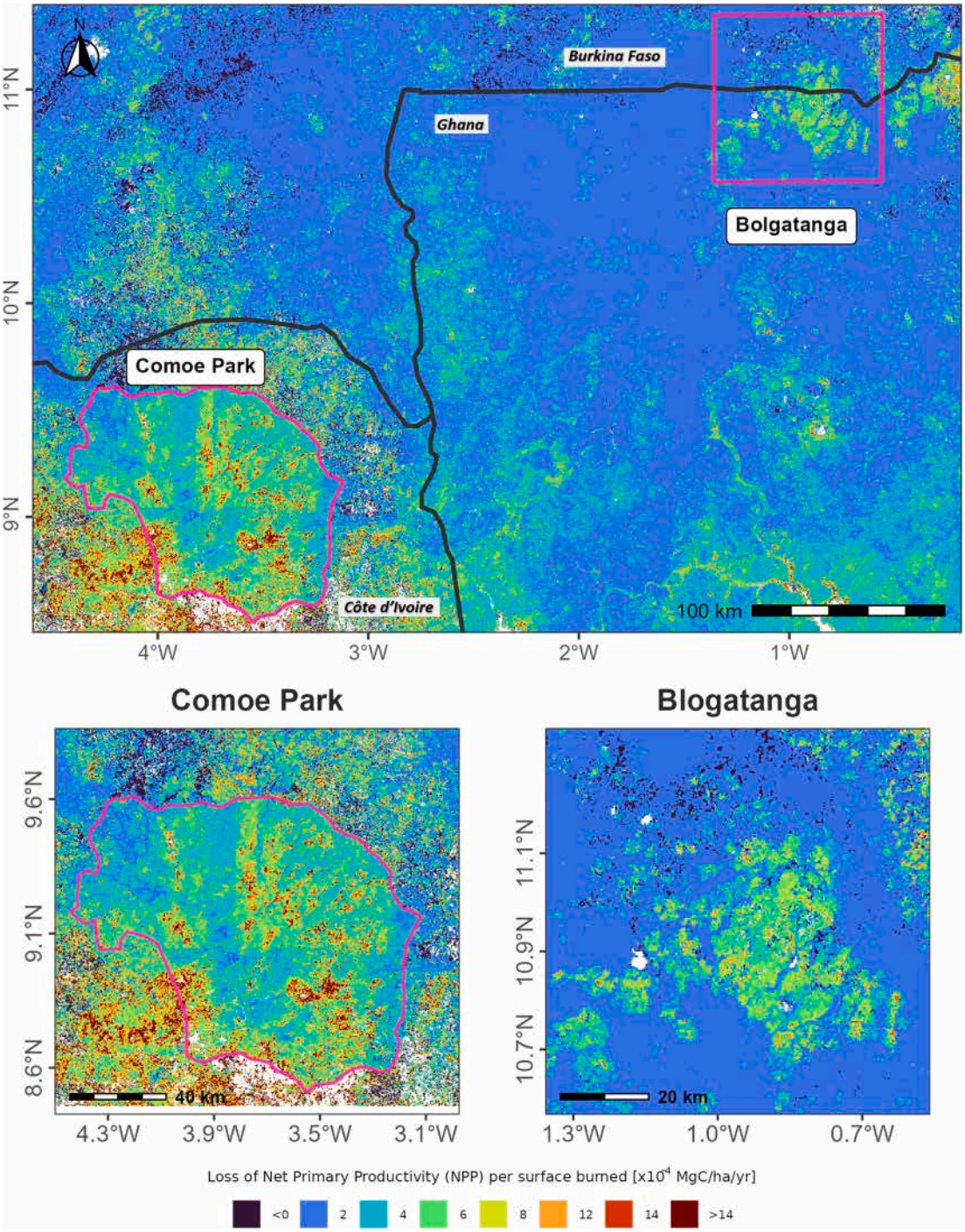

Fig. 7. Net Primary Productivity (NPP) loss density (×10^{-4} Mg C ha^{-1} burned) across the study area. Cooler colours represent lower carbon loss per unit of burned area, while warmer colours indicate areas with higher NPP loss per hectare, reflecting more severe fire impact. Notably, Comoé National Park shows localized hotspots of high loss density, whereas much of the northern savanna exhibits relatively lower per-area NPP loss.

fluctuations, there is no clear long-term change in fire-related carbon loss over 2014–2023. This stability suggests that any potential intensification of fire impact due to climate or land-use changes has so far been offset by other factors (or vice versa). On average, we estimate that wildfires reduced the region's annual NPP by roughly 4–6 % each year (given typical NPP values for these savannas).

Spatially, fire impacts on NPP exhibited a north–south gradient (Fig. 6c). In the northernmost Sudanian savannas (drier region), many areas showed negligible or even slightly positive NPP change despite burning. In about 20 % of the area (mainly North Burkina and extreme North Ghana), NPP in burned pixels was unchanged or a small net gain (up to $+ 0.2 \times 10^2$ Mg C ha^{-1} per year). This counterintuitive gain could occur if post-fire regrowth in wet years overshot the pre-fire biomass or if fires removed mostly dead litter, spurring new growth. The central savanna belt and southern woodland mosaic had moderate NPP losses (up to $\sim 3 \times 10^2$ Mg C ha^{-1} per year). These zones, covering ~ 40 % (central) and ~ 36 % (south) of the area, correspond to mixed land cover where fire removes grass and some woody biomass but ecosystems are moderately resilient. The highest NPP losses were concentrated in about 4–5 % of the area, notably in and around Comoé National Park (southeast of the study area) and parts of southeast Ghana. These areas lost up to $\sim 9 \times 10^2$ Mg C ha^{-1} per year over the decade indicating intense fires in carbon-rich environments (woodland/forest patches). Comoé, for instance, contains dense tree cover in gallery forests that, when burned, result in substantial carbon emission and slow regrowth. This pattern aligns with well-established fire ecology theory: more humid, high-biomass systems tend to suffer greater immediate carbon losses due to the combustion of accumulated fuel loads, while more arid zones — with lower biomass — may show minimal loss or even short-term NPP gains following fire, potentially due to reduced competition or nutrient cycling.

NPP loss density.

When normalized by the BA, the NPP loss density (amount of NPP lost per ha burned) also shows a gradient (Fig. 7). On average, each hectare of BA in the northern savannas resulted in a loss of $\sim 4–6 \times 10^{-4}$ Mg C ha^{-1} of NPP, whereas in the southern, denser vegetated areas, each hectare burned lost $> 10 \times 10^{-4}$ Mg C ha^{-1}. The highest loss densities ($>12 \times 10^{-4}$ Mg C ha^{-1}) were in Comoé National Park and surroundings, indicating that when these forest-savanna mosaics burn, they lose a very large amount of productivity relative to the area burned. This is expected as these areas have more biomass and higher productivity to begin with. In contrast, parts of northern Ghana (around Bolgatanga) had lower loss densities ($\sim 6–8 \times 10^{-4}$ Mg C ha^{-1}), meaning fires there, while frequent, impact less carbon per unit area—consistent with those being grass-dominated fires with lower fuel loads. One interpretation is that northern fires could be "surface fires" consuming mostly grasses, which regrow quickly, whereas southern fires may also consume shrubs or young trees, leading to higher carbon impact. These density maps are useful for pinpointing vulnerable areas where fire does disproportionate damage to productivity (edges of forests or protected areas). They also provide a metric for modelers to calibrate fire emission models: e.g., an average of $\sim 8 \times 10^{-4}$ Mg C ha^{-1} lost can be compared to emission factors and biomass estimates in savannas.

Burned Area – NPP Loss – LULC Nexus.

We analysed how the impacts of fire activity and its productivity vary across different LULC classes (Fig. 8). Overall, savannas and forests were the ecosystems most affected by fire. Roughly 44 % of all savanna areas burned at least once during the study period, including ~ 19 % in woody savannas and ~ 25 % in open savannas. Both subtypes are naturally fire-prone, although they differ in vegetation structure.

In forest ecosystems, approximately 41 % of total forest area was affected by fire. Notably, deciduous forests made up the majority of burned forest area (~39 %), while evergreen and mixed forests combined represented only ~ 2 % of forest area burned. This indicates that

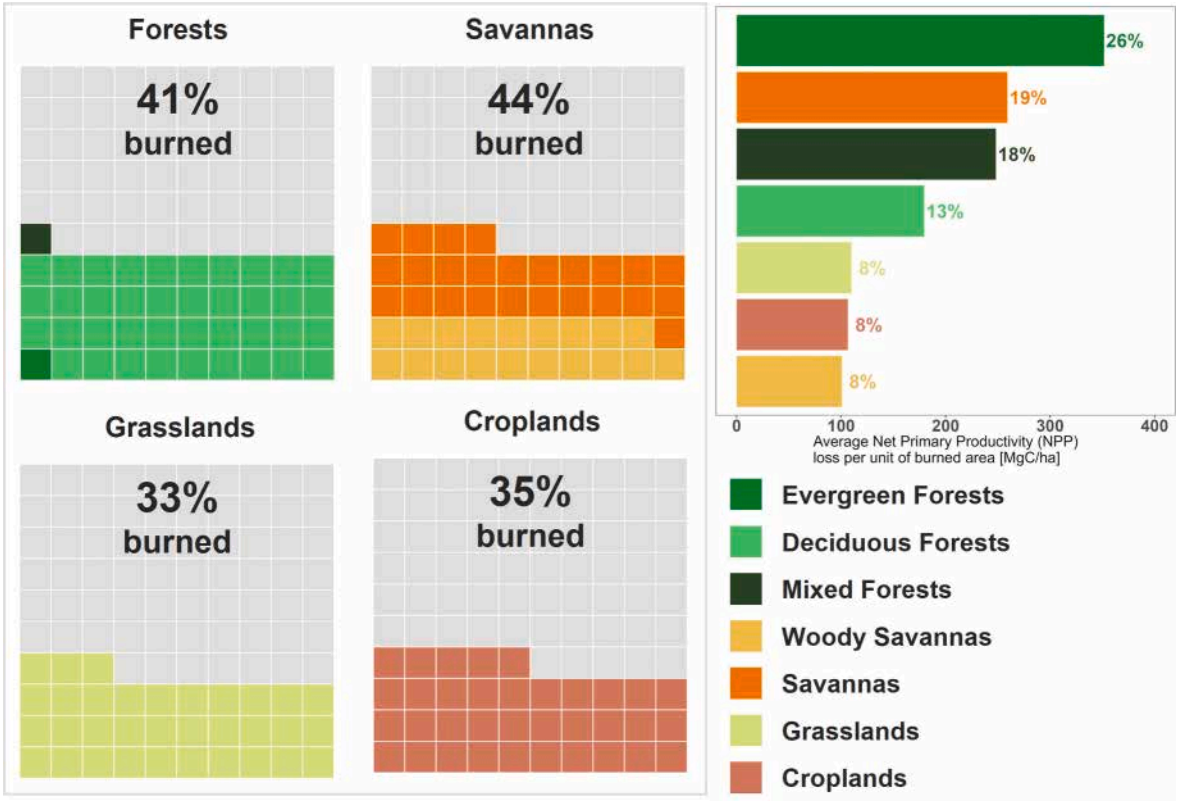

Fig. 8. Burned area and NPP loss by land cover type. Left: Proportion of total burned area occurring in each LULC category (savanna, forest subtypes, cropland, grassland). Right: Proportion of total NPP loss attributable to fires in each LULC. Forest fires (especially evergreen/mixed) yield outsized carbon losses compared to their area burned, whereas grassland/cropland fires have lower impact per area.

even relatively closed deciduous forests can burn extensively during the dry season, whereas evergreen and mixed forests are more fire-resistant due to persistent canopy moisture.

Croplands and grasslands also saw considerable fire activity: about 35 % of cropland area and 33 % of grassland area experienced burning. Fieldwork conducted during the study confirmed that fires in croplands are frequently set intentionally for land preparation or post-harvest residue management. Grassland fires can be natural or used for pasture control. These findings underscore that fire is widespread across both wild and human-managed landscapes in West Africa.

When evaluating the distribution of NPP loss by LULC, clear differences emerge in ecosystem vulnerability:

- in evergreen forests, just ~ 1 % of forest area burned over the whole analysis period, but this small fraction accounted for ~ 26 % of total NPP loss.
- mixed forests had similar proportion: ~1% of area burned, contributing ~ 18 % of NPP loss.
- deciduous forests, with ~ 39 % of forest area burned, caused only ~ 13 % of the NPP loss.

This highlights those fires in evergreen and mixed forests are especially destructive in terms of carbon—they likely kill mature trees and lead to prolonged productivity declines. In contrast, deciduous forests, although more frequently affected, may experience less severe per-area carbon losses due to faster post-fire recovery and more open canopy structure.

Savanna systems exhibited proportional NPP losses: open savannas accounted for ~ 19 %, and woody savannas ~ 8 % of total NPP loss, which aligns closely with their share of BA. These systems, being fire-adapted, tend to regenerate quickly and lose less carbon per hectare burned.

Croplands and grasslands each contributed ~ 8 % of total NPP loss—lower than their respective BA shares—indicating that these systems, with generally low biomass and rapid post-fire regrowth, suffer relatively minor carbon impacts.

5.3. Post-fire vegetation recovery

Recovery trajectories.

Vegetation in most BA eventually regained its pre-fire productivity, but the timeframe for recovery varied widely (Fig. 9). On average, we found that NPP in burned patches returned to baseline in about 3 months post-fire. Notably, roughly 65 % of the burned pixels achieved full recovery within 1 year**.** These quickly recovering areas are largely the grassy savannas and farmlands where either herbaceous vegetation resprouts in the next wet season or crops are replanted. An additional ~ 16 % of BA recovered in 2–3 years. Therefore, by three years out, over 80 % of BA had recovered. The remaining ~ 20 % took longer or did not recover within our analysis period. Specifically, delayed recovery classes (4–5, 6–7, 8–9 years) together accounted for ~ 14 % of BA, and these were mostly scattered in northern Ghana and parts of Comoé National Park. The "very delayed" (8–9 years) category was rare and often corresponded to spots that might have burned multiple times before fully recovering or where a shift in vegetation occurred (e.g., grass replacing shrubs). Fig. 9 highlights that long-term unrecovered patches were not large continuous zones but rather mosaics (small pockets within the generally recovering matrix). For instance, in Comoé National Park, which generally regains productivity in a few years, there were isolated depressions where recovery took nearly the whole decade—possibly due

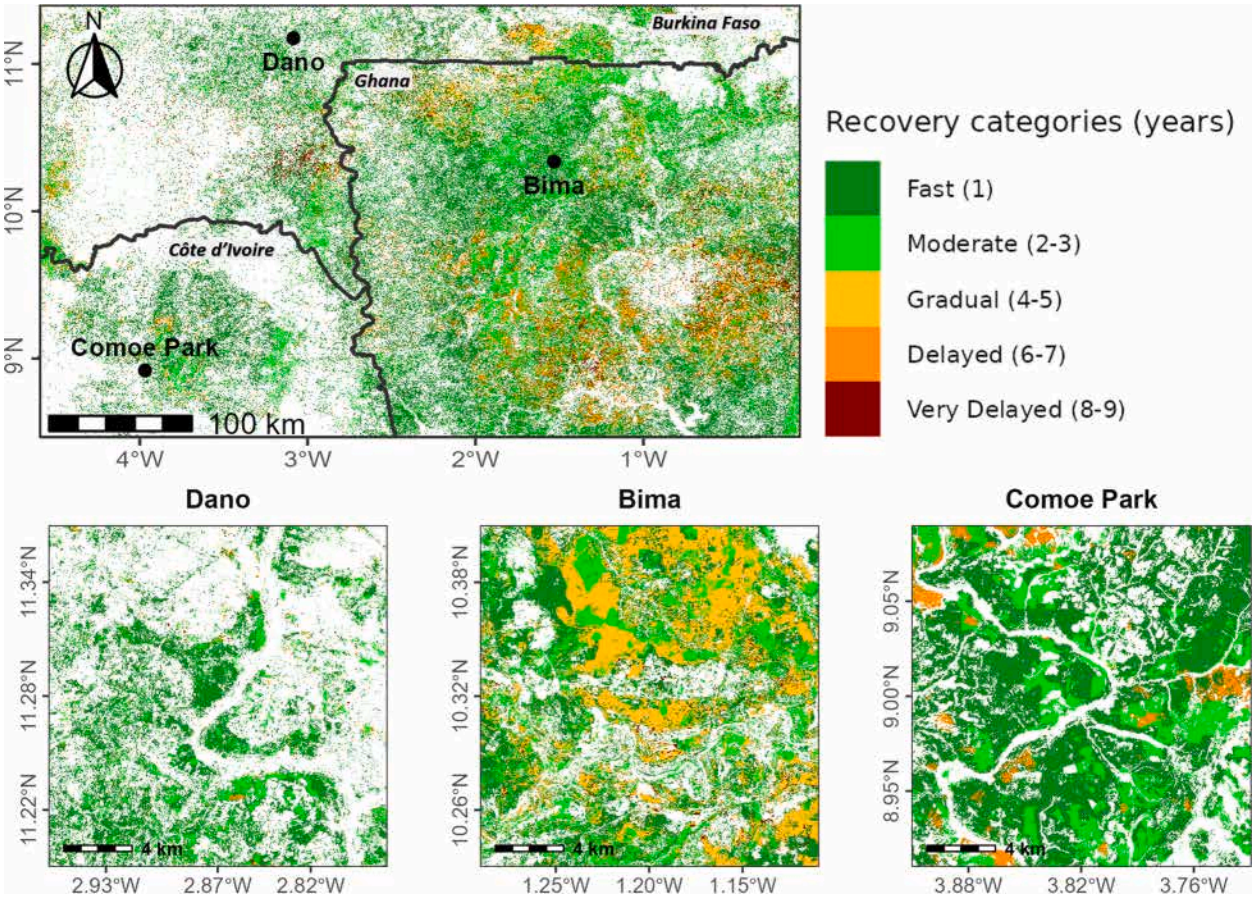

Fig. 9. Post-fire recovery time categories (spatial distribution). Most burnt areas (green) regenerate quickly, whereas scattered patches in Ghana and Comoé National Park (red) show much slower recovery.

to repeated fire hits or drought impacts.

In contrast, some regions like around Dano (Burkina Faso) exhibited very fast recovery, usually within the same growing season or by the next year. These differences suggest that local conditions (soil, species composition, fire intensity) modulate recovery. Overall, the fact that two-thirds of the area bounced back within a year demonstrates a resilient baseline for West African savannas – they are well adapted to frequent fire. However, the presence of a significant minority of areas with multi-year recovery indicates that severe or repeated burns can push some ecosystems to slow regenerative trajectories.

Recovery by land cover.

When analysing recovery rates by LULC, clear patterns emerged (Fig. 10). At monthly scale, grasslands showed the highest proportion of immediate recovery (within 1 month). These are typically areas of pure grasses that can re-sprout quickly from roots after early-season fires, especially if rains return. Deciduous forests, savannas (both woody and open), and croplands had relatively fewer cases of one-month recovery, but many fell into short-term (2–3 months) recovery. Deciduous forests often flush new leaves in the next wet season (within a couple of months after fire if timed before rains), and savannas likewise regrow herbaceous cover by the wet season. Croplands may be ploughed or replanted, effectively "recovering" in terms of productivity when the new crop grows. Medium to long-term recovery (4–7 months) was uncommon overall, but where it occurred it was mostly in savannas and croplands. This could indicate instances of fire coinciding with drought or soil degradation delaying regrowth.

At annual scale, nearly all LULC types were dominated by rapid recovery classes, but with nuanced differences. Deciduous forests actually showed the highest fraction of fast recovery (within 1 year) among LULC categories. This seems counterintuitive given forests have more biomass to regrow; a possible explanation is that many deciduous forest pixels include understory grass that recovers, and the metric NPP might be satisfied by partial recovery of the system (even if tree biomass is not fully restored). Savannas also had a high share of 1-year recoveries, followed by moderate (2–3 year) recoveries. Grasslands and croplands interestingly had more cases of delayed (6–7 years) and very delayed (8–9 years) recovery than forests or savannas. This likely reflects human factors: some croplands might have been abandoned after a fire, or converted to something with lower productivity, hence never "recovering" in terms of NPP. Grassland recovery could be delayed if repeated burning prevents accumulation of biomass year after year. Still, those long delays were a small portion of grassland/cropland pixels.

All vegetation types in this region exhibit strong resilience, but the risk of prolonged recovery is slightly higher in managed or open-land systems, possibly due to land degradation or repeated disturbance, whereas the mostly natural savanna and deciduous woodland systems tend to recover their productivity relatively quickly.

5.4. *Factors influencing recovery rates*

The H2O AutoML analysis selected a GBM as the best model for predicting recovery time from environmental variables. The final GBM achieved high predictive accuracy, with a cross-validated R^2 of approximately 0.94 and a Root Mean Squared Error (RMSE) of 0.5 years, indicating robust model performance. The top-performing GBM slightly outperformed other candidate models, including two additional GBMs with alternative hyperparameters and two XGBoost models.

The variable importance results (Fig. 11), scaled to 100 %, provide clear insights: soil nutrients and soil moisture retention capacity emerged as the most influential predictors, surpassing climatic, land-cover, and fire-related variables. Conversely, fire regime characteristics, soil classification, and vegetation types contributed minimally to explaining recovery variability.

The most important predictor was ***(1) soil total nitrogen***. Areas with higher nitrogen levels recovered more rapidly—likely because nitrogen is a key limiting nutrient that fuels post-fire regrowth. Soils rich in organic nitrogen appear to accelerate the return of biomass and productivity after burning. This was followed by ***(2) soil water-holding capacity*** (measured via retention at 1500 kPa), which ranked among the top variables. Soils with greater water retention sustained vegetation growth better through the dry season, supporting faster recovery independently of rainfall patterns. Both ***(3) NDMI and its interaction with itself*** (NDMI × NDMI) were also highly ranked. This underscores that consistent vegetation moisture—more than just peak greenness—supports resilience. The squared interaction reflects the importance of moisture stability, suggesting that environments with steady moisture availability facilitate stronger recovery than those with fluctuating conditions. Several interaction terms involving ***(4) NDMI and temperature or LST*** were also highly influential. The NDMI × LST term, in particular, highlighted the compound stress of drought and heat: even moist areas may recover slowly under extreme heat due to increased evapotranspiration. Conversely, cooler microclimates aided regrowth

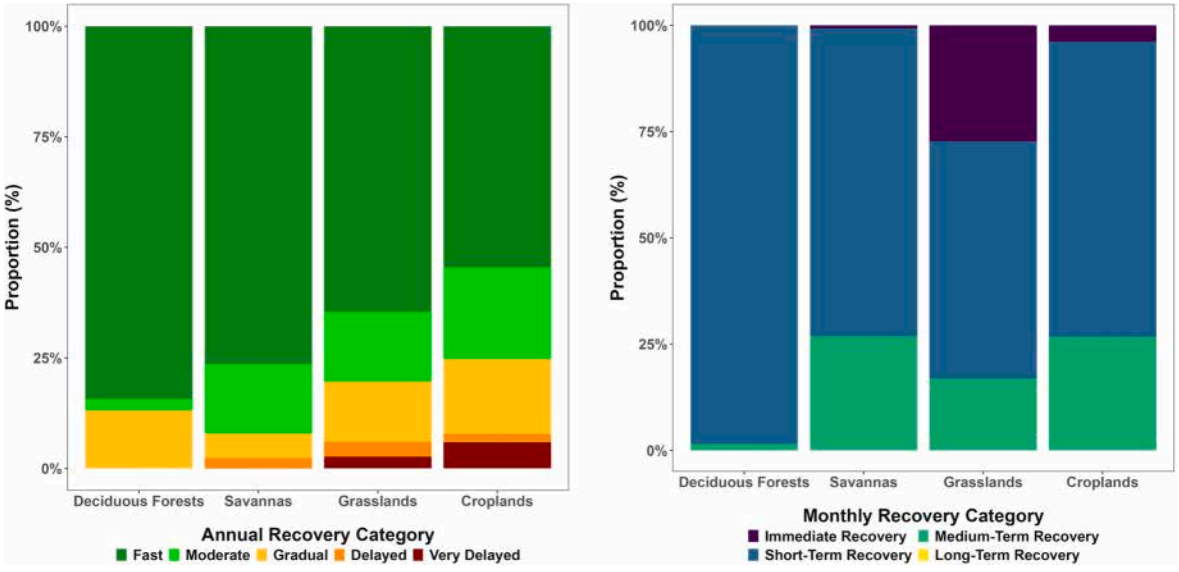

Fig. 10. Recovery patterns by land cover. Left: Proportion of burned area in each LULC achieving annual recovery within 1, 2–3, 4–5, 6–7, 8–9 years. Right: Proportion achieving monthly recovery within 1, 2–3, 4–5, 6–7 months. Grasslands show very fast initial recovery (many in 1 month), while croplands and grasslands have a tail of very delayed cases at the annual scale, unlike forests which mostly recover by 3 years.

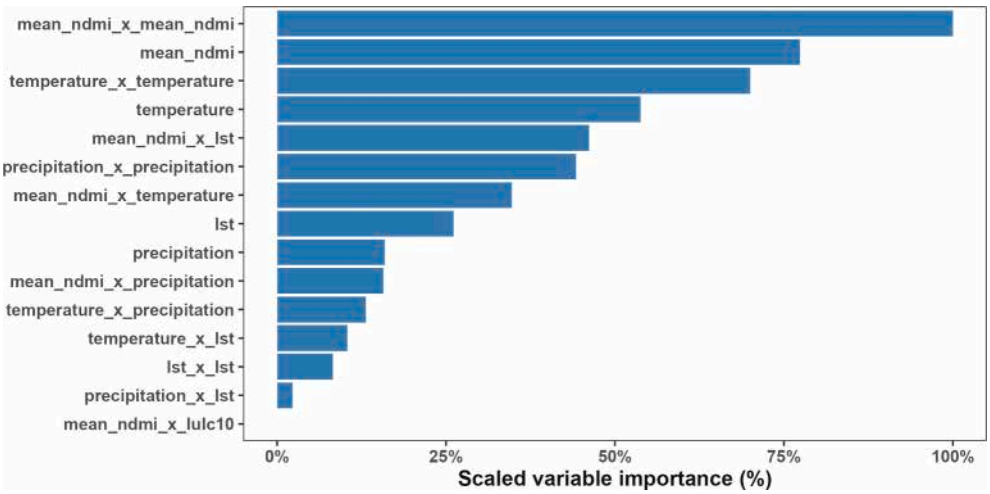

Fig. 11. Variable importance for recovery time (gradient boosting machines – GBM model). Bars show relative importance (% of the top variable). Soil variables (total nitrogen, water-holding capacity) and vegetation moisture (NDMI-related terms) dominate the model, along with their interactions with temperature. Climate × moisture interactions (e.g. NDMI × LST) are also highly influential. Fire frequency and broad land-cover categories have near-zero importance, indicating minor direct effects on recovery.

even in less moist zones. Precipitation and its interactions appeared with lower—but still non-negligible—importance, reinforcing the notion that soil water availability may be more critical than short-term rainfall inputs in supporting regrowth.

By contrast, fire-related variables—such as burn frequency—and vegetation type (land cover class) had near-zero relative importance. Whether a site was grassland or forest, or burned once or multiple times, had limited predictive power once moisture and soil conditions were accounted for. This reinforces the idea that post-fire recovery is primarily shaped by underlying ecosystem traits—not fire recurrence itself.

These results highlight the dominant role of edaphic factors (especially nitrogen availability and soil water retention) in shaping recovery speed. Vegetation moisture (NDMI) and temperature remain important, particularly through their interactions, but nutrient availability and soil hydrological properties substantially enhance model performance. The negligible contribution of fire regime metrics implies that recovery trajectories are largely shaped by ecological context rather than disturbance frequency. While fire characteristics may influence other aspects of fire ecology (e.g. structural change, species turnover), they appear secondary for functional recovery as measured by NPP in this system.

6. Discussion

6.1. Fire regimes and carbon dynamics in west African savannas

Our results paint a comprehensive picture of how wildfire regimes impact vegetation productivity in West African savannas, and they provide important insights into ecosystem resilience. The pronounced seasonality we observed — with fires largely confined to the dry months and peaking in December — aligns with known regional fire regimes (Lehmann et al., 2014; Laris et al., 2016) and reflects the strong influence of climate on fire timing in Africa (Wimberly et al, 2024). However, previous research shows that human land-use practices also shape fire seasonality, often initiating burning earlier than the climate-driven drying cycle would predict (Le Page et al., 2010). While our analysis focused on climatic and environmental drivers, this human dimension is essential for interpreting savanna fire patterns more fully. This seasonal concentration means that fire effects on carbon and ecology are also highly seasonal: a large flush of carbon is released and productivity drops sharply in early dry season, followed by a gradual recovery that often begins even before the onset of rains, likely reflecting early leaf flush and herbaceous regrowth triggered by temperature and photoperiod cues (Herrmann et al., 2005; Ryan et al., 2011). We found no strong long-term trend in BA or NPP loss from 2014 to 2023, suggesting a relatively stable fire regime over the past decade. This is notable because other studies have reported declining BA globally — particularly in African savannas — due to agricultural expansion, grazing pressure, and landscape fragmentation, a phenomenon referred to as the "human fire sink" (Andela et al., 2017). However, more recent work by Caillault et al. (2020) highlights that many savanna regions, especially in West Africa, exhibit stable fire activity over the past decade, where traditional fire use continues and fire suppression is limited. Our study area may reflect this pattern, with fire regimes maintained by customary practices and year-to-year variability shaped primarily by climate rather than fire exclusion. For instance, the dip in fire activity around 2017–2018 coincided with wetter conditions, illustrating how rainfall can override human factors in certain years by limiting fuel dryness.

The integration of high-resolution BA mapping proved crucial for accurately quantifying fire impacts. By capturing small fires, we determined that a considerable portion of the landscape (especially croplands and fragmented savannas) burns at fine scales that coarser satellites miss. These small fires, while individually modest, collectively contributed significantly to total BA and carbon loss. This finding corroborates recent literature emphasizing the importance of accounting for "missing small fires" in global fire budgets (van der Werf et al., 2017; Li et al., 2018). In West African rural contexts, these small burns often result from farm cleaning or hunting activities. The spatial burn frequency patterns we found – with most areas burning only occasionally and very few burning annually – suggest that fire rotation periods are on the order of 3–5 years in many savannas. This is consistent with ecological understanding that while savanna grasses can burn yearly, intentional fire management and patchiness usually create a mosaic of different burn ages (Archibald et al., 2009). Comoé National Park displays a mosaic of fire frequencies: while much of the park burns at moderate intervals, localized zones within it show some of the highest fire recurrence in the region. This suggests that while natural barriers (e.g., rivers, moist forest patches) and management may reduce widespread reburning, certain areas remain highly fire-exposed—possibly due to fuel continuity or anthropogenic ignition within or near park boundaries.

Our analysis of carbon productivity loss due to fire reveals both the scale and ecological pattern of its impact. Across the $\sim$ 230,000 km^2 study region, fires caused an average loss of $\sim 11 \times 10^2$ Mg C ha^{-1} per

year in NPP – carbon that would otherwise have been sequestered in biomass or soil. While savannas are often described as "fire-resilient," this resilience refers primarily to vegetation cover, not carbon balance. The carbon cost of fire is unevenly distributed: more humid, high-biomass areas – such as forest–savanna mosaics and evergreen woodlands – suffer disproportionately high NPP losses per hectare. These systems burn more intensely and recover more slowly, particularly when fire kills woody vegetation that took years to accumulate. This pattern aligns with the fire trap or Gulliver effect (Bond and van Wilgen, 1996), where frequent fires in mesic savannas suppress tree maturation and reinforce open structures despite high productivity. In contrast, semi-arid savannas are more water-limited and less affected per fire (Sankaran et al., 2005; Higgins et al., 2007). Our LULC-stratified results confirm that evergreen forests contribute disproportionately to NPP loss, relative to their BA. This has important implications for carbon management: protecting woody patches and preventing fire intrusion into forest fragments could significantly reduce emissions – even if open savannas and croplands continue to experience regular burning, where carbon is often regained more quickly. This also ties into the broader debate around fire timing and carbon outcomes – namely, whether promoting early dry-season burning could help reduce long-term carbon loss. While our study does not explicitly assess fire timing, the observed resilience of open savannas and vulnerability of woody zones suggests that fire intensity and vegetation type jointly influence carbon dynamics.

Compared to other ecosystems globally, the fire-induced NPP losses observed in West Africa (up to $\sim 9 \times 10^2$ Mg C ha^{-1} per year in forest–savanna mosaics) are high. In southern African savannas and the Brazilian Cerrado, annual fire-driven losses typically range from 2 to 10 Mg C ha^{-1}, reflecting lower biomass and more frequent but less intense fires (Williams et al., 2025; Silva et al., 2019). In contrast, tropical rainforest fires, though rare, can cause catastrophic losses exceeding 50 Mg C ha^{-1} per event due to dense biomass and slow recovery (Aragão et al., 2018). Boreal forests experience similar magnitudes during severe fires, but with long fire-return intervals. These comparisons position West Africa's Forest–savanna transition as a globally significant hotspot for fire-related carbon loss, combining the flammability of savannas with the biomass vulnerability of tropical forests.

Another key point is that we did not observe a significant long-term trend in NPP loss – meaning fire's impact on regional carbon storage has been relatively steady in recent years. However, if climate change leads to more extreme droughts or higher temperatures, one might expect larger NPP losses per fire (as vegetation would be more stressed and perhaps less productive even before fire). Additionally, if socio-economic changes lead to either more intense burning (e.g., through deforestation fires) or less burning (fire suppression), the carbon balance could shift. In this sense, our results provide a baseline for the current decade. Continuous monitoring is needed to detect any deviation from this baseline under future climate scenarios.

6.2. *Vegetation resilience and post-fire recovery processes*

The estimated speed of post-fire recovery — with over 65 % of BA regaining pre-fire NPP within a year — highlights the capacity of many West African savanna ecosystems for rapid functional rebound. This reflects broad fire-adaptive traits among dominant vegetation types, including fast-growing grasses and resprouting woody species (Staver et al., 2011, Zeitler et al., 2025). However, this resilience is not uniform: as our results show, recovery is slower in more humid and woody zones, where fire may inflict greater structural damage and regrowth is delayed. These contrasting dynamics underscore that savannas are both fire-adapted and fire-sensitive, depending on vegetation structure, fuel load, and burn conditions — a complexity also highlighted in recent synthesis work (Lehmann et al., 2014; Hahn and Leßmeister, 2021; Bowring et al., 2022). Our finding that deciduous forests often recovered to pre-fire NPP levels within a year suggests that, while above-ground vegetation may have been altered, root systems likely remained intact, allowing for rapid regrowth and leaf flushing in the next wet season. However, this does not imply full structural or ecological recovery. It is critical to distinguish functional recovery—the return of NPP—from structural recovery, which involves the regrowth of original biomass, canopy structure, and species composition. An area may regain its carbon uptake quickly through fast-growing grasses or resprouting shrubs, yet take years to recover its original tree height, woody biomass, or floristic identity (Bond and Keeley, 2005). Our study focuses on this functional aspect, which is central to understanding carbon cycling, but it does not capture biodiversity shifts or long-term vegetation structure. These may diverge significantly, particularly in zones that burn frequently or intensely, and should be addressed in future work using structural or floristic indicators.

The small fraction of areas with very delayed or no recovery raises important questions. These zones were often located in croplands and grasslands, where land use decisions and agro-pastoral practices, rather than fire alone, may explain the observed low productivity. In these systems, fields may be left fallow, rotated with different crops, or used seasonally for grazing. While fallow land is reportedly declining, it remains a common management strategy. In such cases, our NPP-based analysis would classify these fields as "non-recovered," even if the apparent inactivity reflects intentional land-use choices rather than ecological degradation. Similarly, repeated grazing or clearing pressure may lead to vegetation shifts toward lower-productivity cover types (e.g., compacted soils or unpalatable shrubs).

In more natural systems (especially unmanaged grasslands and open savannas), the pattern of long-term non-recovery may reflect the cumulative effects of repeated burning. While a single fire is often quickly absorbed by fire-adapted vegetation, chronic fire disturbance over years or decades can degrade ecosystems. Frequent burns may reduce soil nutrient stocks (through volatilization or erosion) and favour fire-tolerant but less productive species, ultimately lowering the landscape's carbon carrying capacity (Cleary et al., 2010; Wright et al., 2020). In our data, such processes may appear as areas that never return to pre-fire NPP levels. From a management perspective, identifying these persistent low-productivity patches could help target interventions such as reseeding, grazing exclusion, soil restoration, or adjusted fire regimes to support full ecosystem recovery.

When it comes to the drivers of post-fire recovery, edaphic factors overwhelmingly control recovery speed. Soil fertility and moisture—especially nitrogen content and water-holding capacity—are the strongest predictors of how fast burned savannas bounce back. In contrast, NDMI (post-fire greenness) and temperature rank secondary, while fire frequency and cover type have negligible influence. This suggests that within each land cover type, there is a wide range of recovery outcomes depending on local environmental conditions. However, since fire timing was not included in the analysis, we interpret this result cautiously—fire seasonality may interact with both vegetation type and climate, influencing post-fire recovery.

Another key finding from the drivers analysis was the surprisingly small effect of fire frequency on post-fire recovery time. Intuitively, one might expect areas that burn repeatedly to recover more slowly due to cumulative disturbance. However, our data showed no strong correlation: areas burning for the third or fourth time often recovered as quickly as those burning for the first time, after accounting for environmental variables. This aligns with extensive savanna fire ecology literature, which suggests that frequent burning in fire-adapted systems—particularly mesic savannas—does not necessarily impair recovery and may even maintain vegetation in a stable state (Laris, 2017; Sankaran et al., 2005; Staver et al., 2011).

Recovery in our study area is largely resource-limited: soils rich in nutrients and moisture support fast regrowth and allow woody plants to thrive. This dynamic reflects what has been described as the Gulliver effect or fire trap (Freeman et al., 2017; Hoffmann et al., 2019), where frequent low-intensity fires suppress tree recruitment but do not reduce

grass productivity—keeping ecosystems locked in a low-biomass, fast-recovering state. Many grasslands in our study area are likely adapted to this regime, where fast-regrowing annuals dominate and repeated fire is part of the natural cycle.

In contrast, on nutrient-poor or well-drained soils, tree seedlings remain stunted. This is consistent with theories suggesting that chronic burning depletes soil nitrogen and suppresses NPP. Ecologically, our findings support the idea that the tree–grass balance in savannas hinges not just on fire regime but also on soil fertility and water availability, which control juvenile growth rates (Pellegrini et al., 2018). For land management, these findings imply that improving soil resources can speed recovery: for example, conserving soil organic matter or lengthening fire-free intervals (especially after late-season burns) can help trees reach escape height. In water-retentive, nutrient-rich soils, vegetation can recover rapidly even under frequent fire.

It is also possible that the range of fire frequencies in our dataset (mostly ≤ 7 burns over 10 years) was not sufficient to detect degradation thresholds. More extreme cases of high-frequency burning, or longer historical periods, might show different outcomes. Additionally, our recovery metric resets after each fire, meaning a pixel can recover quickly each time, even if its absolute productivity remains lower over time. This highlights an important nuance: rapid "recovery" to a modest baseline in a fire-adapted grassland is not the same as structural or compositional recovery in more woody systems.

While prior work such as Tepley et al. (2018) highlights the role of vegetation feedbacks and recovery duration in forested systems, our findings suggest that in West African savannas, post-fire recovery as measured by NPP is more strongly governed by climate and soil conditions than by fire frequency or land cover. This likely reflects the faster recovery dynamics and lower sensitivity to vegetation-fire feedbacks in these fire-adapted landscapes.

6.3. Implications for fire management and ecosystem conservation

Our findings have several implications for fire management and climate mitigation in West African savannas. One key result is that forested areas exhibited higher per-hectare NPP losses during fire events, even though many functionally recovered within a year. This suggests that while these systems are capable of regaining carbon uptake, they may still experience significant immediate biomass loss and potential shifts in structure or species composition. Forest patches embedded within the savanna matrix—especially those with dense woody cover—are therefore ecologically sensitive and merit targeted protection from high-intensity or repeated burning.

Fire management strategies in protected areas such as Comoé National Park should prioritize preventing late dry-season fires, when fuels are driest and fire intensity peaks. Effective approaches may include maintaining firebreaks, promoting early dry-season burns in surrounding savannas to reduce fuel loads, and engaging with local communities who already practice seasonally timed burning for agricultural and pastoral purposes. As noted by Laris (2017), early burning is often used traditionally to protect rather than harm forested zones, and suppression of these practices can backfire by increasing the risk of intense late-season burns. Supporting community-led fire calendars—rather than imposing top-down restrictions—offers a culturally grounded, ecologically effective path toward resilience. This not only helps to minimize carbon emissions but also preserves biodiversity in forest remnants that may host species not found in the surrounding savanna.

Our results also show that most savanna fires have relatively low long-term impacts on productivity, particularly when burning occurs under milder conditions. This supports a fire management paradigm that views fire not as a threat to be eradicated, but as a tool to be timed and guided wisely. Controlled early-season burns, when vegetation still retains moisture, appear to allow for faster recovery and reduced carbon loss—patterns reflected in our monthly recovery data. Rather than replacing traditional fire use, fire management policies should aim to enhance its effectiveness and sustainability, by co-developing strategies that support both local land use objectives and broader ecological goals such as soil conservation or carbon sequestration.

From a climate change perspective, maintaining productivity and reducing carbon losses in frequently burned savanna systems is a meaningful contribution to regional mitigation strategies. Though savannas store less carbon per hectare than rainforests, they cover vast areas and burn regularly—making their cumulative role in the carbon cycle non-trivial. Reducing unnecessary or unintentional fires—especially those offering little benefit or caused by unmanaged ignition—can help cut emissions. At the same time, supporting rapid post-fire recovery through landscape restoration, soil moisture retention (e.g., mulching, cover crops), or erosion control may accelerate carbon re-sequestration.

Finally, although our study did not find strong trends in fire activity or recovery over the past decade, this does not guarantee future stability. Climate projections for West Africa point toward more erratic rainfall patterns and potentially longer or harsher dry seasons (Alamou et al., 2022; Yapo et al., 2023). If these changes lead to earlier or more intense fires, NPP losses could rise, and recovery may slow. Conversely, elevated CO_2 levels could enhance plant growth through fertilization effects (O'Leary et al., 2015), potentially speeding up recovery or fuelling more intense burns if biomass accumulates. Continued monitoring using high-resolution fire and productivity metrics, as demonstrated in this study, will be critical for anticipating and responding to shifts in fire regimes under changing climate conditions.

6.4. Uncertainties and limitations

While comprehensive, our study has several uncertainties and limitations worth noting. First, our BA mapping, despite its high resolution, is not infallible. We relied on remote sensing detection, which can miss understory fires or very small burns, especially under cloud cover. We mitigated this with multi-source data and our algorithm, but an unknown fraction of area might still be unaccounted for (particularly fires occurring under dense smoke or in persistently cloudy periods). The validation against BARD was limited to 2019, expansion of reference data in other years would strengthen confidence in our BA estimates.

Second, satellite-derived NPP has its own uncertainties. We downscaled annual NPP using GPP fractions, assuming a proportional relationship. If fires themselves alter the efficiency of NPP vs. GPP (for example, maybe plants under post-fire stress have higher respiration fraction), our estimated NPP loss might be off. Also, MODIS at 500 m could mix burned and unburned areas in one pixel, and while we tried to isolate burned contributions by masking with our BA map, any misregistration or mixed pixel issues could blur the actual NPP drop. We included October and May in the fire-season integration to capture full effects, but it is possible that some pre-fire productivity decline (e.g., due to drought) or post-fire fertilization effects are conflated. Field measurements of biomass and NPP after fires would be valuable to calibrate the magnitude of satellite-inferred losses.

Our recovery metric, based on matching pre-fire NPP, might sometimes label a pixel as "recovered" even if the vegetation composition changed. For example, if a forest burns and is replaced by fast-growing shrubs/grass that achieve similar NPP, we count it as recovered, even though from a biodiversity standpoint it is not the same. Conversely, if fire causes a shift to a less productive state (like shrubland to grassland with lower leaf area), we count as non-recovery even if ground cover is back. Thus, our method is focused on functional recovery and does not capture all ecological dimensions of recovery. This should be kept in mind – managers should not equate "NPP recovery" with full ecosystem recovery.

There are several limitations and uncertainties in our driver's analysis that need to be addressed. One significant limitation is that the analysis does not establish causality. Although the statistical performance of the driver's analysis is robust, correlations between variables

such as soil nutrients, moisture, temperature, and recovery should be interpreted with caution. It is important to note that while soil fertility (nitrogen content) and moisture availability were found to be strong predictors of post-fire recovery, other unmeasured factors—such as soil microbial activity, herbivory, and other ecological processes—could also play a role in shaping recovery outcomes. Thus, while soil factors like nitrogen and water retention capacity provide key insights, further field studies are necessary to better isolate the exact mechanisms driving recovery.

Another limitation arises from our use of environmental proxies, such as NDMI and temperature, which may not fully capture the complexity of the recovery process. For instance, NDMI captures moisture availability but may not accurately represent soil moisture at deeper levels or reflect finer-scale temporal variations in soil water content. Although NDMI is a valuable indicator, it is still a remote-sensing-derived metric, and its interpretation could be affected by seasonal changes and vegetation type. Future studies should consider combining multiple moisture proxies, such as direct soil moisture measurements, to improve the accuracy of moisture availability assessments, especially in heterogeneous landscapes like those of West African savannas.

Fire seasonality was another aspect not fully incorporated into the analysis. While our study focused on the impacts of fire in the dry season, the timing of the fire (early vs. late dry season) could influence both fire intensity and the capacity of ecosystems to recover (Laris et al., 2021). Fire seasonality, along with its interactions with temperature and moisture, may modulate recovery dynamics. The absence of fire timing in our current analysis represents an important gap, as late-season fires often burn more intensely, which could lead to higher carbon loss and slower recovery. In future studies, incorporating fire seasonality and fire intensity data—possibly through satellite-derived fire radiative power or field data on fire severity—would offer a more comprehensive understanding of how fire interacts with the environment to affect post-fire recovery.

Finally, while we used a range of climate and soil data, some critical environmental variables could not be included. For example, soil data, such as from the SoilGrids dataset (Batjes and van Oostrum, 2023), provide valuable insights into the influence of soil properties on recovery at a 250 m resolution. However, higher-resolution data would be preferable to better capture finer-scale variations in soil properties, especially in heterogeneous landscapes like West African savannas. Furthermore, our climate predictors came from coarse-resolution reanalysis data (ERA5 $\sim$ 10 km), which may not capture fine-scale rainfall variability (e.g., localized storms) that also influences recovery. Nevertheless, the relatively strong performance of our models, even with these broad-scale inputs, suggests that soil data and temperature are dominant and detectable drivers of post-fire resilience.

The inclusion of more detailed soil data in future studies could refine our understanding of how these factors influence recovery time, particularly in areas where soil moisture and fertility interact with climate to modulate regrowth. Furthermore, our climate predictors came from coarse-resolution reanalysis data (ERA5 $\sim$ 10 km), which may not capture fine-scale rainfall variability (e.g., localized storms) that also influences recovery. Nevertheless, the relatively strong performance of our models, even with these broad-scale inputs, suggests that edaphic factors, soil moisture and temperature are dominant and detectable drivers of post-fire resilience.

Finally, future research could extend this work by examining emissions (translating NPP loss to carbon emissions and accounting for combustion vs. decay) and by integrating faunal impacts (fires also impact wildlife and grazing, which in turn affect vegetation recovery). There is also the need to consider extreme events: our decade had no exceptionally severe drought. If an extreme El Niño drought occurred, what would be the combined effect with fire? Our study sets the stage for answering such questions by providing methods and baseline relationships.

7. Conclusion

We developed and applied an integrated remote sensing framework to estimate how fires affect ecosystem productivity and recovery in West African savannas. By using high-resolution satellite data (VIIRS, Landsat, Sentinel-2) and machine learning, we produced a 30 m BA record and captured detailed fire impacts on carbon dynamics from 2014 to 2023. Our findings reveal a generally resilient yet fire-influenced landscape: most areas burn infrequently and recover their productivity within months, reflecting adaptive traits of savanna vegetation. On the other hand, intense fires in high-biomass areas (like forest patches) cause substantial carbon losses and longer recovery, highlighting those areas as priorities for fire management. We showed that soil factors, especially soil nutrients (e.g., total nitrogen) and soil moisture retention capacity, overwhelmingly govern the pace of post-fire recovery, more so than fire history or vegetation type. This recovery reflects the ecosystem's ability to regain its carbon uptake capacity after fire, as captured through NPP trajectories. However, this does not equate to full ecological recovery, which would require species-level monitoring of vegetation composition and structure. This emphasizes the need to incorporate climate projections in fire impact assessments – e.g., prolonged droughts could impede recovery even if fire regimes remain unchanged. From a practical perspective, this study underscores the importance of fine-scale fire monitoring in savannas. The ability to detect small fires allowed us to more accurately estimate BA and NPP loss, which are crucial for carbon budget calculations. We estimate that, over the last decade, fires reduced NPP in the region by roughly 11×10^{-2} Mg C ha^{-1} per year. Mitigating these carbon losses through improved fire management (optimizing fire timing and location) could contribute to climate change mitigation, while also protecting local livelihoods and biodiversity.

For instance, preventing late-season fires in and around forests can avoid disproportionately large carbon emissions and foster quicker vegetation rebound.

We also provide new methodological avenues – our two-tailed BA detection and the use of AutoML for ecological modelling can be transferred to other regions and disturbance studies. This multidisciplinary approach (combining earth observation, ecology, and data science) proved powerful in unravelling complex interactions between fire, climate, and vegetation.

In conclusion, West African savannas exhibit rapid but variable recovery from fire. While functional resilience, in terms of NPP recovery, provides insight into the ecosystem's ability to bounce back, it does not necessarily imply full ecological recovery, which can involve slower processes like biomass and canopy regrowth. Sustainable management will require maintaining that recovery capacity in the face of growing human pressures and climate change. By identifying the drivers of recovery and the areas of concern, our research offers a science-based guide for policymakers and land managers. Actions such as integrated fire management planning, conservation of moisture-rich refugia, and community engagement in fire use can enhance post-fire recovery and safeguard the ecosystem services these savannas provide – from carbon sequestration to biodiversity and agriculture. As wildfires globally are becoming a focal point under climate change, this regional study contributes a timely case of how remote sensing can inform proactive strategies to coexist with fire while minimizing its adverse impacts.

CRediT authorship contribution statement

Boris Ouattara: Writing – review & editing, Writing – original draft, Software, Methodology, Formal analysis, Data curation, Conceptualization. **Michael Thiel:** Writing – review & editing, Validation, Supervision, Project administration, Funding acquisition. **Gerald Forkuor:** Writing – review & editing, Methodology, Investigation, Data curation. **Florent Mouillot:** Writing – review & editing, Investigation, Data curation. **Paul Laris:** Writing – review & editing, Methodology, Investigation, Conceptualization. **Ebagnerin Jérôme Tondoh:** Writing –

review & editing, Investigation, Data curation. **Barbara Sponholz:** Writing – review & editing, Validation, Supervision, Investigation.

Declaration of competing interest

The authors declare that they have no known competing financial interests or personal relationships that could have appeared to influence the work reported in this paper.

Acknowledgements

The authors acknowledge the support from the German Federal Ministry of Education and Research (BMBF) via the project carrier at the German Aerospace Center (DLR Projektträger) through the research projects: WASCAL-DE-Coop (FKZ: 01LG1808A) and NetCDA (FKZ: 01LG2301A).

All datasets used in this study are publicly available from established repositories:

- VIIRS active fire detections (VNP14IMGML): https://firms.modaps.eosdis.nasa.gov (Last access January 2025)
- Harmonized Landsat–Sentinel imagery (HLS): https://cmr.earthdata.nasa.gov/stac/ (Last access January 2025)
- MODIS NPP/GPP (MxD17A2H/MxD17A3H) and land cover (MCD12Q1): accessible via Google Earth Engine (Last access January 2025)
- ERA5 climate variables: accessible via Google Earth Engine (Last access January 2025)
- SoilGrids250m (ISRIC): https://www.isric.org/explore/isric-soil-data-hub (Last access January 2025)
- Burned Area Reference Database (BARD): https://edatos.consorciomadrono.es/dataverse/BARD (Last access January 2025)

We also compared our burned area maps against publicly available reference products, including:

- FireCCI51 (MODIS, 250 m; Chuvieco et al., 2018)
- FireCCI SFD20 (Sentinel-2, 20 m; Chuvieco et al., 2022)
- FireCCI S310 (Sentinel-3, 300 m; Lizundia-Loiola et al., 2022)
- MCD64A1 (MODIS, 500 m; Giglio et al., 2018)
- Prototype VIIRS-BA dataset (375 m; Ouattara et al., 2024)

These products were used as independent references for evaluation. Full citations are provided in the References section.

The code and processed data supporting this study are available from the corresponding author upon reasonable request.

Data availability

The authors do not have permission to share data.

References

Alamou, A.E., Obada, E., Biao, E.I., Zandagba, E.B.J., Da-Allada, C.Y., Bonou, F., Baloïtcha, E., Tilmes, S., Irvine, P., 2022. Impact of Stratospheric Aerosol Geoengineering on Meteorological Droughts in West Africa. Atmos. 13 (2), 234. https://doi.org/10.3390/atmos13020234.

Amoako, E.E., Gambiza, J., 2022. Fire Use Practices, Knowledge and Perceptions in a West African Savanna Parkland. PLoS One. https://doi.org/10.1371/journal.pone.0240271.

Andela, N., Morton, D.C., Giglio, L., Yang, C., van der Werf, G.R., Kasibhatla, P.S., DeFries, R., Collatz, G.J., Hantson, S., Kloster, S., Bachelet, D., Forrest, M., Lasslop, G., Li, F., Mangeon, S., Melton, J.R., Ye, C., Randerson, J.T., 2017. A Human-Driven Decline in Global burned Area. Science. https://doi.org/10.1126/science.aal4108.

Aragão, L.E.O.C., Anderson, L.O., Fonseca, M.G., Rosan, T.M., Vedovato, L.B., Wagner, F., Silva, C.V.J., Silva, C.H.L., Arai, E., Aguiar, A.P., Barlow, J., Berenguer, É., Deeter, M.N., Domingues, L.G., Gatti, L.V., Gloor, M., Malhi, Y., Marengo, J., Miller, J.B., Saatchi, S., 2018. 21st Century Drought-Related fires Counteract the Decline of Amazon deforestation Carbon Emissions. Nat. Commun. 9 (1). https://doi.org/10.1038/s41467-017-02771-y.

Archibald, S., Roy, D.P., van Wilgen, B.W., Scholes, R.J., 2009. What Limits Fire? an Examination of Drivers of Burnt Area in Southern Africa. Glob. Chang. Biol. https://doi.org/10.1111/j.1365-2486.2008.01754.x.

Atak, B.K., Tonyaloğlu, E.E., 2020. Monitoring the Spatiotemporal changes in Regional Ecosystem Health: a Case Study in Izmir, Turkey. Environ. Monit. Assess. 192 (6). https://doi.org/10.1007/s10661-020-08357-4.

Batjes, N. H., & van Oostrum, A. J. M. (2023). World Soil Information Service (WoSIS) - Procedures for standardizing soil analytical method descriptions (Issue ISRIC Report 2023/01). Doi: 10.17027/isric-1dq0-1m83.

Beale, C.M., Mustaphi, C.J.C., Morrison, T.A., Archibald, S., Anderson, T.M., Dobson, A. P., Donaldson, J.E., Hempson, G.P., Probert, J., Parr, C.L., 2018. Pyrodiversity Interacts with Rainfall to increase Bird and Mammal Richness in African Savannas. Ecol. Lett. 21 (4), 557–567. https://doi.org/10.1111/ele.12921.

Beckage, B., Ellingwood, C., 2009. Fire Feedbacks with Vegetation and Alternative Stable States. Complex Systems 18 (1), 159–173. https://doi.org/10.25088/complexsystems.18.1.159.

Bond, W.J., Keeley, J.E., 2005. Fire as a Global 'Herbivore': the Ecology and Evolution of Flammable Ecosystems. Trends Ecol. Evol. 20 (7), 387–394. https://doi.org/10.1016/j.tree.2005.04.025.

Bond, W.J., van Wilgen, B.W., 1996. Fire and Plants. Springer, Netherlands. https://doi.org/10.1007/978-94-009-1499-5.

Bowring, S., Jones, M.W., Ciais, P., Guenet, B., Abiven, S., 2022. Pyrogenic Carbon Decomposition critical to Resolving Fire's Role in the Earth System. Nat. Geosci. 15 (2), 135–142. https://doi.org/10.1038/s41561-021-00892-0.

Bradter, U., Altringham, J.D., Kunin, W.E., Thom, T., O'Connell, J., Benton, T.G., 2022. Variable Ranking and selection with Random Forest for Unbalanced Data. Environ. Data Sci. 1. https://doi.org/10.1017/eds.2022.34.

Caillault, S., Laris, P., Fleurant, C., Delahaye, D., Ballouche, A., 2020. Anthropogenic fires in West African Landscapes: a Spatially Explicit Model Perspective of Humanized Savannas. Fire 3 (4), 62. https://doi.org/10.3390/fire3040062.

Calderisi, G., Rossetti, I., Cogoni, D., Fenu, G., 2025. Delayed Vegetation Mortality after Wildfire: Insights from a Mediterranean Ecosystem. Plants 14 (5), 730. https://doi.org/10.3390/plants14050730.

Claverie, M., Ju, J., Masek, J.G., Dungan, J.L., Vermote, E.F., Roger, J.-C., Skakun, S.V., Justice, C., 2018. The Harmonized Landsat and Sentinel-2 surface reflectance data set. Remote Sens. Environ. 219, 145–161. https://doi.org/10.1016/j.rse.2018.09.002.

Chen, Y., Hall, J., van Wees, D., Andela, N., Hantson, S., Giglio, L., van der Werf, G.R., Morton, D.C., Randerson, J.T., 2023. Multi-Decadal Trends and Variability in burned Area from the Fifth Version of the Global Fire Emissions Database (GFED5). Earth Syst. Sci. Data 15 (11), 5227–5259. https://doi.org/10.5194/essd-15-5227-2023.

Chuvieco, E., Lizundia-Loiola, J., Pettinari, M.L., Ramo, R., Padilla, M., Tansey, K., Mouillot, F., Laurent, P., Storm, T., Heil, A., Plummer, S., 2018. Generation and analysis of a new global burned area product based on MODIS 250 m reflectance bands and thermal anomalies. Earth Syst. Sci. Data 10 (4), 2015–2031. https://doi.org/10.5194/essd-10-2015-2018.

Chuvieco, E., Martín, M.P., Palacios, A., 2002. Assessment of Different Spectral Indices in the Red-Near-Infrared Spectral Domain for burned Land Discrimination. Int. J. Remote Sens. https://doi.org/10.1080/01431160210153129.

Chuvieco, E., Roteta, E., Sali, M., Stroppiana, D., Boettcher, M., Kirches, G., Storm, T., Khairoun, A., Pettinari, M.L., Franquesa, M., Albergel, C., 2022. Building a small fire database for Sub-Saharan Africa from Sentinel-2 high-resolution images. Sci. Total Environ. 845. https://doi.org/10.1016/j.scitotenv.2022.157139.

Cleary, M.B., Pendall, E., Ewers, B.E., 2010. Aboveground and Belowground Carbon Pools after Fire in Mountain big Sagebrush Steppe. Rangel. Ecol. Manage. 63 (2), 187–196. https://doi.org/10.2111/rem-d-09-00117.1.

Dahan, K.S., Kasei, R.A., Husseini, R., 2023. Contribution of Remote Sensing to Wildfire Trend and Dynamic Analysis in two of Ghana's Ecological zones: Guinea-Savanna and Forest-Savanna Mosaic. Fire Ecol. 19 (1). https://doi.org/10.1186/s42408-023-00198-z.

Devine, A., Stott, I., McDonald, R.A., Maclean, I.M.D., 2015. Woody Cover in Wet and Dry <scp>A</Scp>frican Savannas after six decades of Experimental fires. J. Ecol. 103 (2), 473–478. https://doi.org/10.1111/1365-2745.12367.

Devineau, J., Fournier, A., Nignan, S., 2010. Savanna Fire Regimes Assessment with MODIS Fire Data: their Relationship to Land Cover and Plant Species distribution in Western Burkina Faso (West Africa). J. Arid Environ. 74 (9), 1092–1101. https://doi.org/10.1016/j.jaridenv.2010.03.009.

Dezfuli, A., Ichoku, C., Bosilovich, M.G., 2024. Large-Scale climate Features Control Fire Emissions and Transport in Africa. Geophys. Res. Lett. https://doi.org/10.1029/2024gl110179.

Dikshit, A., Evans, J.P., 2024. Quantifying Vegetation Recovery after Fire considering Post-Fire Rainfall. Environ. Res. Commun. 6 (12), 121501. https://doi.org/10.1088/2515-7620/ad9dbd.

Dimobe, K., Tondoh, J., Weber, J.C., Bayala, J., Ouédraogo, K., Greenough, K.M., 2018. Farmers' Preferred tree Species and their potential Carbon stocks in Southern Burkina Faso: Implications for Biocarbon Initiatives. PLoS One 13 (12), e0199488. https://doi.org/10.1371/journal.pone.0199488.

Dwomoh, F.K., Wimberly, M.C., 2017. Fire Regimes and their Drivers in the Upper Guinean Region of West Africa. Remote Sens. (Basel) 9 (11), 1117. https://doi.org/10.3390/rs9111117.

EOSDIS. (2025). NASA CMR-STAC API. https://cmr.earthdata.nasa.gov/stac/.

Ermida, S.L., Soares, P.C., Mantas, V., Göttsche, F., Trigo, I.F., 2020. Google Earth Engine Open-Source Code for Land Surface Temperature Estimation from the Landsat Series. Remote Sens. (Basel) 12 (9), 1471. https://doi.org/10.3390/rs12091471.

Fernández-García, V., Santamarta, M., Fernández-Manso, A., Quintano, C., Marcos, E., Calvo, L., 2018. Burn Severity Metrics in Fire-Prone Pine Ecosystems along a Climatic Gradient using Landsat Imagery. Remote Sens. Environ. 206, 205–217. https://doi.org/10.1016/j.rse.2017.12.029.

Filipponi, F., 2019. Exploitation of Sentinel-2 Time Series to Map burned areas at the National Level: a Case Study on the 2017 Italy Wildfires. In Remote Sensing. https://doi.org/10.3390/rs11060622.

FIRMS. (2025). Fire Information for Resource Management System (FIRMS) - Providing Active Fire Data for Near-Real Time Monitoring and Applications. https://firms.modaps.eosdis.nasa.gov/.

Forkel, M., Dorigo, W., Lasslop, G., Chuvieco, E., Hantson, S., Heil, A., Teubner, I., Thonicke, K., Harrison, S.P., 2019. Recent global and regional trends in burned area and their compensating environmental controls. Environ. Res. Commun. 1 (5), 051005. https://doi.org/10.1088/2515-7620/ab25d2.

Freeman, M.E., Vesk, P.A., Murphy, B.P., Cook, G.D., Richards, A.E., Williams, R.J., 2017. Defining the Fire Trap: Extension of the Persistence Equilibrium Model in Mesic Savannas. Austral Ecol. 42 (8), 890–899. https://doi.org/10.1111/aec.12516.

Friedl, M., & Sulla-Menashe, D. (2019). MCD12Q1 MODIS/Terra+Aqua Land Cover Type Yearly L3 Global 500m SIN Grid V006 . NASA EOSDIS Land Processes DAAC.

Fryda, T., LeDell, E., Gill, N., Aiello, S., Fu, A., Candel, A., Click, C., Kraljevic, T., Nykodym, T., Aboyoun, P., Kurka, M., Malohlava, M., Poirier, S., & Wong, W. (2024). h2o: R Interface for the "H2O" Scalable Machine Learning Platform. R package version 3.44.0.3. https://CRAN.R-project.org/package=h2o.

Fu, Y., Li, R., Wang, X., Bergeron, Y., Valeria, O., Chavardès, R.D., Wang, Y., Hu, J., 2020. Fire Detection and Fire Radiative Power in Forests and Low-Biomass Lands in Northeast Asia: MODIS Versus VIIRS Fire Products. Remote Sens. (Basel) 12 (18), 2870. https://doi.org/10.3390/rs12182870.

Gaveau, D., Descals, A., Salim, M.A., Sheil, D., Sloan, S., 2021. Refined Burned-Area Mapping Protocol using Sentinel-2 Data increases Estimate of 2019 Indonesian burning. Earth Syst. Sci. Data 13 (11), 5353–5368. https://doi.org/10.5194/essd-13-5353-2021.

van Gerrevink, M.J., Veraverbeke, S., 2021. Evaluating the Near and Mid Infrared Bi-Spectral Space for Assessing Fire Severity and Comparison with the Differenced Normalized Burn Ratio. Remote Sens. (Basel) 13 (4), 695. https://doi.org/10.3390/rs13040695.

Giglio, L., Boschetti, L., Roy, D.P., Humber, M.L., Justice, C.O., 2018. The Collection 6 MODIS burned area mapping algorithm and product. Remote Sens. Environ. 217 (September), 72–85. https://doi.org/10.1016/j.rse.2018.08.005.

Giglio, L., Schroeder, W., Justice, C.O., 2016. The collection 6 MODIS active fire detection algorithm and fire products. Remote Sens. Environ. 178, 31–41. https://doi.org/10.1016/j.rse.2016.02.054.

Gold, Z.J., Pellegrini, A.F.A., Refsland, T., Andrioli, R.J., Bowles, M.L., Brockway, D.G., Burrows, N., Franco, A.C., Hallgren, S.W., Hobbie, S.E., Hoffmann, W.A., Kirkman, K., Reich, P.B., Savadogo, P., Silvério, D.V., Stephan, K., Strydom, T., Varner, J.M., Wade, D.D., Staver, A.C., 2023. Herbaceous Vegetation responses to Experimental Fire in Savannas and Forests Depend on Biome and climate. Ecol. Lett. 26 (7), 1237–1246. https://doi.org/10.1111/ele.14236.

Google Developpers. (2024). Resampling - Google Earth Engine. Google. https://developers.google.com/earth-engine/guides/resample.

Hahn, K., & Leßmeister, A. (2021). Sustainable Use of Savanna Vegetation in West Africa in the Context of Climate and Land Use Change. In: Nachhaltige Entwicklung in einer Gesellschaft des Umbruchs. 45–64. Doi: 10.1007/978-3-658-31466-8_4.

Herrmann, S., Anyamba, A., Tucker, C.J., 2005. Recent Trends in Vegetation Dynamics in the African Sahel and their Relationship to climate. Glob. Environ. Chang. 15 (4), 394–404. https://doi.org/10.1016/j.gloenvcha.2005.08.004.

Hersbach, H., Bell, B., Berrisford, P., Hirahara, S., Horányi, Á., Muñoz-Sabater, J., Nicolas, J.P., Peubey, C., Radu, R., Schepers, D., Simmons, A.J., Soci, C., Abdalla, S., Abellan, X., Balsamo, G., Bechtold, P., Biavati, G., Bidlot, J., Bonavita, M., Thépaut, J., 2020. The ERA5 Global Reanalysis. Q. J. R. Meteorolog. Soc. 146 (730), 1999–2049. https://doi.org/10.1002/qj.3803.

Higgins, S.I., Bond, W.J., February, E.C., Bronn, A., Euston-Brown, D., Enslin, B., Govender, N., Rademan, L., O'Regan, S., Potgieter, A.L.F., Scheiter, S., Sowry, R., Trollope, L.A., Trollope, W.S.W., 2007. Effects of four decades of Fire Manipulation on Woody Vegetation Structure in Savanna. Ecology 88 (5), 1119–1125. https://doi.org/10.1890/06-1664.

Hijmans, R. J. (2025). terra: Spatial Data Analysis. R package version 1.8-56. https://github.com/rspatial/terra.

Hoffmann, W.A., Geiger, E.L., Gotsch, S.G., Rossatto, D.R., Silva, L.C.R., Lau, O.L., Haridasan, M., Franco, A.C., 2012. Ecological Thresholds at the Savanna-forest Boundary: how Plant Traits, Resources and Fire govern the distribution of Tropical Biomes. Ecol. Lett. 15 (7), 759–768. https://doi.org/10.1111/j.1461-0248.2012.01789.x.

Hoffmann, W.A., Sanders, R.W., Just, M.G., Wall, W.A., Hohmann, M.G., 2019. Better Lucky than good: how Savanna Trees Escape the Fire Trap in a Variable World. Ecology 101 (1). https://doi.org/10.1002/ecy.2895.

Huntley, B. (2023). The Ecological Role of Fire. 149–165. Doi: 10.1007/978-3-031-18923-4_7.

Hurteau, M.D., Liang, S., Westerling, A.L., Wiedinmyer, C., 2019. Vegetation-Fire Feedback Reduces projected Area burned under climate Change. Sci. Rep. 9 (1). https://doi.org/10.1038/s41598-019-39284-1.

Jones, G.M., Tingley, M.W., 2021. Pyrodiversity and Biodiversity: a history, Synthesis, and Outlook. Divers. Distrib. 28 (3), 386–403. https://doi.org/10.1111/ddi.13280.

Justice, C.O., Román, M.O., Csiszar, I., Vermote, E.F., Wolfe, R.E., Hook, S.J., Friedl, M., Wang, Z., Schaaf, C.B., Miura, T., Tschudi, M., Riggs, G., Hall, D.K., Lyapustin, A.I., Devadiga, S., Davidson, C., Masuoka, E.J., 2013. Land and cryosphere products from Suomi NPP VIIRS: Overview and status. J. Geophys. Res. Atmos. 118 (17), 9753–9765. https://doi.org/10.1002/jgrd.50771.

Katagis, T., Gitas, I.Z., 2022. Assessing the Accuracy of MODIS McD64a1 C6 and FireCCI51 burned Area Products in Mediterranean Ecosystems. Remote Sens. (Basel) 14 (3), 602. https://doi.org/10.3390/rs14030602.

Key, C., & Benson, N. (1999). Measuring and remote sensing of burn severity: the CBI and NBR (L. Neuenschwander & K. Ryan, Eds.). Joint Fire Science Conference and Workshop, vol. II. http://jfsp.nifc.gov/conferenceproc/index.htm.

Key, C.H., Benson, N.C., 2006. LA-1 Landscape Assessment (LA) Sampling and Analysis Methods. USDA Forest Service Gen. Tech. Rep. RMRS-GTR-164-CD, 2006.

Klupar, I., Rocha, A.V., Rastetter, E.B., 2021. Alleviation of Nutrient Co-limitation Induces Regime Shifts in Post-fire Community Composition and Productivity in Arctic Tundra. Glob. Chang. Biol. 27 (14), 3324–3335. https://doi.org/10.1111/gcb.15646.

Koné, N.A., Silué, K.S., Konaté, S., Linsenmair, K.E., 2018. Determinants of Termite Assemblages' Characteristics within Natural Habitats of a Sudano-Guinean Savanna (Comoe National Park, Côte D'Ivoire). Insects 9 (4), 189. https://doi.org/10.3390/insects9040189.

Krawchuk, M.A., Moritz, M.A., 2011. Constraints on global fire activity vary across a resource gradient. Ecology 92 (1), 121–132. http://www.jstor.org/stable/29779580.

Landi, M.A., Di Bella, C.M., Bravo, S., Bellis, L.M., 2020. Structural Resistance and Functional Resilience of the Chaco Forest to Wildland fires: an Approach with MODIS Time Series. Austral Ecol. 46 (2), 277–289. https://doi.org/10.1111/aec.12977.

Laris, P., 2005. Spatiotemporal problems with detecting and mapping mosaic fire regimes with coarse-resolution satellite data in savanna environments. Remote Sens. Environ. 99 (4), 412–424. https://doi.org/10.1016/j.rse.2005.09.012.

Laris, P., 2011. Humanizing Savanna Biogeography: linking Human Practices with Ecological patterns in a frequently burned Savanna of Southern Mali. Ann. Assoc. Am. Geogr. 101 (5), 1067–1088. https://doi.org/10.1080/00045608.2011.560063.

Laris, P. (2017). Managing a Burned Mosaic: A Landscape-scale Human Ecological Model of Savanna Fires in Mali. In Savannas and Dry Forests (pp. 155–186). Routledge. Doi: 10.4324/9781315243788-7.

Laris, P., Dadashi, S., Jo, A., Wechsler, S.P., 2016. Buffering the Savanna: Fire Regimes and Disequilibrium Ecology in West Africa. Plant Ecol. 217 (5), 583–596. https://doi.org/10.1007/s11258-016-0602-0.

Laris, P., Jacobs, R., Koné, M., Dembélé, F., Rodrigue, C.M., 2020. Determinants of fire intensity in working landscapes of an african savanna. Fire Ecol. 16 (27), 16. https://doi.org/10.1186/s42408-020-00085-x.

Laris, P., Koné, M., Dembélé, F., Yang, L., Jacobs, R., 2021. Methane Gas Emissions from Savanna fires: what Analysis of local burning Regimes in a Working West African Landscape tell Us. Biogeoscience 18, 6229–6244. https://doi.org/10.5194/bg-18-6229-2021.

Laris, P., Koné, M., Dembélé, F., Rodrigue, C.M., Yang, L., Jacobs, R., Laris, Q., Camara, F., 2023. The Pyrogeography of methane Emissions from Seasonal Mosaic burning Regimes in a West African Landscape. Fire 6 (2), 52. https://doi.org/10.3390/fire6020052.

Le Page, Y., Oom, D., Silva, J.M.N., Jönsson, P., Pereira, J.M.C., 2010. Seasonality of Vegetation fires as Modified by Human Action: observing the Deviation from Eco-climatic Fire Regimes. Glob. Ecol. Biogeogr. 19 (4), 575–588. https://doi.org/10.1111/j.1466-8238.2010.00525.x.

Lehmann, C.E.R., Anderson, T.M., Sankaran, M., Higgins, S.I., Archibald, S., Hoffmann, W.A., Hanan, N.P., Williams, R.J., Fensham, R.J., Felfili, J.M., Hutley, L. B., Ratnam, J., José, J.S., Montes, R., Franklin, D.C., Russell-Smith, J., Ryan, C.M., Durigan, G., Hiernaux, P., Bond, W.J., 2014. Savanna Vegetation-Fire-climate Relationships Differ among Continents. Science 343 (6170), 548–552. https://doi.org/10.1126/science.1247355.

Li, F., Zhang, X., Kondragunta, S., Csiszar, I., 2018. Comparison of Fire Radiative Power estimates from VIIRS and MODIS Observations. J. Geophys. Res. Atmos. 123 (9), 4545–4563. https://doi.org/10.1029/2017JD027823.

Liu, J., Maeda, E.E., Wang, D., Heiskanen, J., 2021. Sensitivity of Spectral Indices on burned Area Detection using Landsat Time Series in Savannas of Southern Burkina Faso. Remote Sens. (Basel) 13 (13), 2492. https://doi.org/10.3390/rs13132492.

Lizundia-Loiola, J., Franquesa, M., Khairoun, A., Chuvieco, E., 2022. Global burned area mapping from Sentinel-3 Synergy and VIIRS active fires. Remote Sens. Environ. 282. https://doi.org/10.1016/j.rse.2022.113298.

Marcos, E., Fernández-García, V., Fernández-Manso, A., Quintano, C., Valbuena, L., Tárrega, R., Luis-Calabuig, E., Calvo, L., 2018. Evaluation of Composite Burn Index and Land Surface Temperature for Assessing Soil Burn Severity in Mediterranean Fire-Prone Pine Ecosystems. Forests 9 (8), 494. https://doi.org/10.3390/f9080494.

Masek, J., Ju, J., Roger, J., Skakun, S., Vermote, E., Claverie, M., Dungan, J., Yin, Z., Freitag, B., & Justice, C. (2021a). HLS Operational Land Imager Surface Reflectance and TOA Brightness Daily Global 30m v2.0. NASA EOSDIS Land Processes Distributed Active Archive Center.

Masek, J., Ju, J., Roger, J., Skakun, S., Vermote, E., Claverie, M., Dungan, J., Yin, Z., Freitag, B., & Justice, C. (2021b). HLS Sentinel-2 Multi-spectral Instrument Surface Reflectance Daily Global 30m v2.0. NASA EOSDIS Land Processes Distributed Active Archive Center. Doi: 10.5067/HLS/HLSS30.002.

McLeod, A.I., 2011. Kendall: Rank Correlation and Permutation Procedures. R Package Version 2, 2. https://cran.r-project.org/web/packages/Kendall/index.html.

Murphy, S.W., de Souza Filho, C.R., Wright, R., Sabatino, G., Correa Pabon, R., 2016. HOTMAP: Global hot target detection at moderate spatial resolution. Remote Sens. Environ. 177, 78–88. https://doi.org/10.1016/j.rse.2016.02.027.

N'Dri, A.B., Gignoux, J., Dembélé, A., Konaté, S., 2012. Short Term Effects of Fire Intensity and Fire Regime on Vegetation Dynamic in a Tropical Humid Savanna

(Lamto, Central Côte D'Ivoire). Nat. Sci. 04 (12), 1056–1064. https://doi.org/10.4236/ns.2012.412134.
N'Dri, A.B., Kpangba, K.P., Werner, P.A., Koffi, K.F., Bakayoko, A., 2022. The Response of Sub-adult Savanna Trees to six Successive annual fires: an Experimental Field Study on the Role of Fire season. J. Appl. Ecol. 59 (5), 1347–1361. https://doi.org/10.1111/1365-2664.14149.
O'Leary, G.J., Christy, B., Nuttall, J.G., Huth, N., Cammarano, D., Stöckle, C., Basso, B., Shcherbak, I., Fitzgerald, G.J., Luo, Q., Farre-Codina, I., Palta, J.A., Asseng, S., 2015. Response of wheat growth, grain yield and water use to elevated CO2 under a Free-Air CO2 Enrichment (FACE) experiment and modelling in a semi-arid environment. Glob. Chang. Biol. 21 (7), 2670–2686. https://doi.org/10.1111/gcb.12830.
Olson, D.M., Dinerstein, E., Wikramanayake, E., Burgess, N., Powell, G.V.N., Underwood, E.C., Jennifer, A., Itoua, I., Strand, H.E., Morrison, J., Allnutt, T.F., Ricketts, T.H., Kura, Y., Lamoreux, J.F., Hedao, P., Kassem, K.R., 2001. Terrestrial Ecoregions of the World: a New Map of Life on Earth. Bioscience 51 (11), 933–938. https://doi.org/10.1641/0006-3568(2001)051[0933:teotwa]2.0.co;2.
Ouattara, B., Thiel, M., Sponholz, B., Paeth, H., Yebra, M., Mouillot, F., Kacic, P., Hackman, K., 2024. Enhancing burned area monitoring with VIIRS dataset: a case study in Sub-Saharan Africa. Sci. Remote Sens. 10. https://doi.org/10.1016/j.srs.2024.100165.
Pellegrini, A.F.A., Ahlström, A., Hobbie, S.E., Reich, P.B., Nieradzik, L.P., Staver, A.C., Scharenbroch, B.C., Jumpponen, A., Anderegg, W.R.L., Randerson, J.T., Jackson, R. B., 2018. Fire frequency drives decadal changes in soil carbon and nitrogen and ecosystem productivity. Nature 553 (7687), 194–198. https://doi.org/10.1038/nature24668.
Pellegrini, A.F.A., Pringle, R.M., Govender, N., Hedin, L.O., 2016. Woody Plant Biomass and Carbon Exchange Depend on Elephant-fire Interactions across a Productivity Gradient in African Savanna. J. Ecol. 105 (1), 111–121. https://doi.org/10.1111/1365-2745.12668.
Pinto, M.M., Trigo, R.M., Trigo, I.F., DaCamara, C.C., 2021. A Practical Method for High-Resolution burned Area monitoring using Sentinel-2 and VIIRS. Remote Sens. (Basel) 13 (9), 1608. https://doi.org/10.3390/rs13091608.
Ramo, R., Roteta, E., Bistinas, I., van Wees, D., Bastarrika, A., Chuvieco, E., van der Werf, G.R., 2021. African burned area and fire carbon emissions are strongly impacted by small fires undetected by coarse resolution satellite data. Proc. Natl. Acad. Sci. 118 (9), 1–7. https://doi.org/10.1073/pnas.2011160118.
Roques, K.G., O'Connor, T.G., Watkinson, A.R., 2001. Dynamics of Shrub Encroachment in an African Savanna: Relative Influences of Fire, Herbivory, Rainfall and Density Dependence. J. Appl. Ecol. 38 (2), 268–280. https://doi.org/10.1046/j.1365-2664.2001.00567.x.
Rossetti, I., Calderisi, G., Cogoni, D., Fenu, G., 2024. Post-Fire Vegetation (Non-)recovery across the Edges of a Wildfire: an Unexplored Theme. Fire 7 (7), 250. https://doi.org/10.3390/fire7070250.
Rossetti, I., Cogoni, D., Calderisi, G., Fenu, G., 2022. Short-Term Effects and Vegetation Response after a Megafire in a Mediterranean Area. Land 11 (12), 2328. https://doi.org/10.3390/land11122328.
Roteta, E., Bastarrika, A., Ibisate, A., Chuvieco, E., 2021. A preliminary global automatic burned-area algorithm at medium resolution in google earth engine. Remote Sens. (Basel) 13 (21). https://doi.org/10.3390/rs13214298.
Running, S.W., Nemani, R.R., Heinsch, F.A., Zhao, M., Reeves, M.C., Hashimoto, H., 2004. A Continuous Satellite-Derived measure of Global Terrestrial Primary production. Bioscience. https://doi.org/10.1641/0006-3568(2004)054[0547:acsmog]2.0.co;2.
Ryan, C.M., Williams, M., Grace, J., 2011. Above- and Belowground Carbon stocks in a Miombo Woodland Landscape of Mozambique. Biotropica 43 (4), 423–432. https://doi.org/10.1111/j.1744-7429.2010.00713.x.
Sankaran, M., Hanan, N.P., Scholes, R.J., Ratnam, J., Augustine, D.J., Cade, B.S., Gignoux, J., Higgins, S.I., Le Roux, X., Ludwig, F., Ardo, J., Banyikwa, F., Bronn, A., Bucini, G., Caylor, K.K., Coughenour, M.B., Diouf, A., Ekaya, W., Feral, C.J., Zambatis, N., 2005. Determinants of woody cover in african savannas. Nature 438 (7069), 846–849. https://doi.org/10.1038/nature04070.
Schroeder, W., Oliva, P., Giglio, L., Csiszar, I.A., 2014. The New VIIRS 375m active fire detection data product: Algorithm description and initial assessment. Remote Sens. Environ. 143, 85–96. https://doi.org/10.1016/j.rse.2013.12.008.
Shang, R., Zhu, Z., Zhang, J., Qiu, S., Yang, Z., Li, T., Yang, X., 2022. Near-Real-Time monitoring of Land Disturbance with Harmonized Landsats 7–8 and Sentinel-2 Data. Remote Sens. Environ. 278, 113073. https://doi.org/10.1016/j.rse.2022.113073.
Silva, A. B., Pessi, D. D., Dantas-junior, A. B., Rosa, D. F., Cardoso-silva, H., Musso, C., Sanchez, G. F., Henke-oliveira, C., Diego, P., Oliveira, S. De, Setzer, A., Setzer, A., Morelli, F., Souza, J. C., Angelica, A., Casella, C., Palmeira, A. F., Setzer, A., Morelli, F., & Marques, A. R. (2019). 7th International Wildland Fire Conference – Wildfire 2019 of Fire Management Policies.
Staver, A.C., Archibald, S., Levin, S.A., 2011. Tree Cover in Sub-Saharan Africa: Rainfall and Fire Constrain Forest and Savanna as Alternative Stable States. Ecology 92 (5), 1063–1072. https://doi.org/10.1890/10-1684.1.
Storey, E.A., Stow, D.A., O'Leary, J.F., 2016. Assessing postfire recovery of chamise chaparral using multi-temporal spectral vegetation index trajectories derived from Landsat imagery. Remote Sens. Environ. 183, 53–64. https://doi.org/10.1016/j.rse.2016.05.018.
Stroppiana, D., Sali, M., Busetto, L., Boschetti, M., Ranghetti, L., Franquesa, M., Pettinari, M.L., Chuvieco, E., 2022. Sentinel-2 sampling design and reference fire perimeters to assess accuracy of burned Area products over Sub-Saharan Africa for the year 2019. ISPRS J. Photogramm. Remote Sens. 191 (September), 223–234. https://doi.org/10.1016/j.isprsjprs.2022.07.015.
Tepley, A.J., Thomann, E., Veblen, T.T., Perry, G.L.W., Holz, A., Paritsis, J., Kitzberger, T., Anderson-Teixeira, K.J., 2018. Influences of Fire–vegetation Feedbacks and Post-fire Recovery rates on Forest Landscape Vulnerability to Altered Fire Regimes. J. Ecol. 106 (5), 1925–1940. https://doi.org/10.1111/1365-2745.12950.
Thapa, S.K., de Jong, J.F., Hof, A.R., Subedi, N., Joshi, L.R., Prins, H.H.T., 2022. Fire and Forage Quality: Postfire Regrowth Quality and Pyric Herbivory in Subtropical Grasslands of Nepal. Ecol. Evol. 12 (4). https://doi.org/10.1002/ece3.8794.
Thuiller, W., 2024. Ecological Niche Modelling. Curr. Biol. 34 (6), R225–R229. https://doi.org/10.1016/j.cub.2024.02.018.
Tredennick, A. T., Karembé, M., Dembélé, F., Dohn, J., & Hanan, N. P. (2014). Weak Effects of Fire, Large Herbivores, and Their Interaction on Regrowth of Harvested Trees in Two West African Savannas. PeerJ PrePrints 2:e718v1, Doi: 10.7287/peerj.preprints.718v1.
Van Der Werf, G.R., Randerson, J.T., Giglio, L., Van Leeuwen, T.T., Chen, Y., Rogers, B. M., Mu, M., Van Marle, M.J.E., Morton, D.C., Collatz, G.J., Yokelson, R.J., Kasibhatla, P.S., 2017. Global fire emissions estimates during 1997-2016. Earth Syst. Sci. Data 9 (2), 697–720. https://doi.org/10.5194/essd-9-697-2017.
Veraverbeke, S., Harris, S., Hook, S., 2011. Evaluating spectral indices for burned area discrimination using MODIS/ASTER (MASTER) airborne simulator data. Remote Sens. Environ. 115 (10), 2702–2709. https://doi.org/10.1016/j.rse.2011.06.010.
Vincent, J., Mihailou, H., Massaro, M., 2024. Post-fire Grazing by Feral Ungulates significantly Reduces Perennial Grass Cover in North Australian Mesic Savannas. Austral Ecol. 49 (12). https://doi.org/10.1111/aec.70018.
Williams, M., Milodowski, D.T., Smallman, T.L., Dexter, K.G., Hegerl, G.C., McNicol, I. M., O'Sullivan, M., Roesch, C.M., Ryan, C.M., Sitch, S., Valade, A., 2025. Precipitation–fire functional interactions control biomass stocks and carbon exchanges across the world's largest savanna. Biogeosciences 22 (6), 1597–1614. https://doi.org/10.5194/bg-22-1597-2025.
Wimberly, M.C., Wanyama, D., Doughty, R., Peiro, H., Crowell, S., 2024. Increasing fire activity in African Tropical Forests is Associated with deforestation and climate Change. Geophys. Res. Lett. 51 (9). https://doi.org/10.1029/2023gl106240.
Wright, J.P., DeLaMater, D.S., Simha, A., Ury, E.A., Ficken, C., 2020. Changes in Prescribed Fire Frequency Alter Ecosystem Carbon Dynamics. Ecosystems 24 (3), 640–651. https://doi.org/10.1007/s10021-020-00540-5.
Wulder, M.A., Hermosilla, T., White, J.C., Hobart, G., Masek, J.G., 2021. Augmenting Landsat Time Series with Harmonized Landsat Sentinel-2 Data Products: Assessment of Spectral Correspondence. Sci. Remote Sens. 4, 100031. https://doi.org/10.1016/j.srs.2021.100031.
Yapo, A.L.M., Kouassi, B.K., Diawara, A., Yoroba, F., Famien, A.M., Touré, P.R., Kouadio, K., Tiemoko, D.T., Sylla, M.B., Diédhiou, A., 2023. Changes in the Seasonal Cycle of Heatwaves, Dry and Wet Spells over West Africa using CORDEX Simulations. Atmos. 14 (10), 1582. https://doi.org/10.3390/atmos14101582.
Zanaga, D., Kerchove, R. Van De, Keersmaecker, W. De, Souverijns, N., Brockmann, C., Quast, R., Wevers, J., Grosu, A., Paccini, A., Vergnaud, S., Cartus, O., Santoro, M., Fritz, S., Georgieva, I., Lesiv, M., Carter, S., Herold, M., Li, L., Tsendbazar, N., … Arinò, O. (2021). ESA WorldCover 10 M 2020 V100. Doi: 10.5281/zenodo.5571936.
Zeitler, E.F., Robertson, K., Dixon, C., Lashley, M.A., 2025. Fire season Differentially Affects Resprouting Vigor of Pyrophytic and Mesophytic Hardwoods in a Southeastern U.S. Pine Savanna. For. Ecol. Manage. 578, 122478. https://doi.org/10.1016/j.foreco.2024.122478.
Zhao, M., Running, S.W., Nemani, R., 2006. Sensitivity of Moderate Resolution Imaging Spectroradiometer (MODIS) Terrestrial Primary production to the Accuracy of Meteorological Reanalyses. J. Geophys. Res. Atmos. 111 (G1). https://doi.org/10.1029/2004jg000004.
Zhu, Z., Woodcock, C.E., 2014. Automated Cloud, Cloud Shadow, and Snow Detection in Multitemporal Landsat Data: an Algorithm Designed specifically for monitoring Land Cover Change. Remote Sens. Environ. https://doi.org/10.1016/j.rse.2014.06.012.
Zoffoun, O.G., Djagoun, C.A.M.S., Nguyen, T.T., Sinsin, B., Sogbohossou, E.A., 2024. Understanding Fire Intensity in the Sudanian Savannah of Western Africa: Implications for Sustainable Fire Management. Afr. J. Ecol. 62 (2). https://doi.org/10.1111/aje.13278.
Zoungrana, A., Visser, M., Cannière, C.D., Ouédraogo, P.C., Bationo, B.A., Traoré, S., 2023. Impact of Agrarian Dynamics on Land Use and Land Cover changes around Protected areas of the Pô-Nazinga-Sissili complex in Burkina Faso. Tropicultura. https://doi.org/10.25518/2295-8010.2280.